DOE/ET/11319--T5

DEVELOPMENT OF MOLTEN-CARBONATE FUEL CELLS FOR POWER GENERATION

Quarterly Progress Report
15 November 1978 through 15 February 1979

Work Performed Under Contract DE-AC03-77ET11319

Prepared for
THE UNITED STATES DEPARTMENT OF ENERGY

Prepared by
General Electric Company
Corporate Research and Development
Schenectady, New York 12301

March 1979

SRD-79-060

DISCLAIMER

DEVELOPMENT OF MOLTEN-CARBONATE

FUEL CELLS FOR POWER GENERATION

Quarterly Progress Report
15 November 1978 through 15 February 1979

AC02-77ET11319

Work Performed Under Contract DE-AC03-77ET11319

Prepared for
THE UNITED STATES DEPARTMENT OF ENERGY

Prepared by
General Electric Company
Corporate Research and Development
Schenectady, New York 12301

March 1979

MGW

Table of Contents

List of Figures

List of Tables

FOREWORD

The work described herein represents a team effort, under the direction of Dr. Deb Chatterji, Manager, Electrochemistry Branch.

Technical and support personnel contributing to the described work include:

Dr. R.H. Arendt	GE/CRD[1]
Mr. M.C. Baker	GE/DECP[2]
Dr. M.W. Breiter	GE/CRD
Dr. K.W. Browall	GE/CRD
Dr. N.S. Choudhury	GE/ESPD[3]
Mr. A.R. Fragala	GE/DECP
Mr. J.W. Harrison	GE/DECP
Mr. E.C. Hayes	GE/CRD
Mr. C.D. Iacovangelo	GE/CRD
Mr. J.F. McElroy	GE/DECP
Mr. F.W. Secor	GE/CRD
Dr. H.S. Spacil	GE/CRD
Dr. J.L. Weininger	GE/CRD
Mr. J.E. Yasi	GE/DECP

[1]General Electric Corporate Research and Development, Schenectady, New York

[2]General Electric Direct Energy Conversion Programs, Wilmington, Massachusetts

[3]General Electric Energy Systems Programs Department, Schenectady, New York

Special mention is made here of the primary authors of specific sections:

Section 2.1	Dr. M.W. Breiter DECP Staff
Section 3	Dr. R.H. Arendt Mr. A.R. Fragala
Section 4	Dr. J.L. Weininger
Section 5	Mr. C.D. Iacovangelo
Section 6	DECP Staff

ABSTRACT

This report describes molten carbonate fuel cell research and development at General Electric Company during the three month period beginning 15 November 1978 and ending 15 February 1979. The objectives of this Phase I effort include the development of promising concepts to circumvent a number of outstanding technical challenges in molten carbonate fuel cell technology and the better definition of the operating limits of molten carbonate fuel cells and power plant based thereupon.

During this quarter of the program, principal activities have been the operation of experimental molten carbonate fuel cells using pure and H_2S- and HCl-contaminated fuels which simulate coal-derived fuels, the development of synthesis and fabrication techniques to prepare electrolyte tiles, the diagnostic analysis of new and used electrolyte tiles, the quantification of anode sintering, the fabrication of a 10"x10" scaled-up single cell, and design activities leading to a stackable 10" x 10" cell.

Specific accomplishments include improvements in the electrode/electrolyte "package" leading to reduced electrode flooding and longer anode life, improved understanding of $LiAlO_2$ morphology changes, the completion of an anode sintering study, and the first results showing the detremental effects of HCl at the cell cathode. Progress was also made in an effort to scale-up tile manufacture to 20" x 20" size and cells to 10" x 10" size.

EXECUTIVE SUMMARY

Experimental Cell Operation

Cell studies were carried out in 3" x 3" laboratory carbonate fuel cells for the purposes of defining cell performance limitations, evaluating new electrode and electrolyte components, and improving cell performance and endurance. Using chromium-stabilized nickel anodes, thinner (15 mil) cathodes, and tiles prepared by the aqueous slurry process, significant improvements were made in previously cited problems of high cell resistance and electrode flooding. However, the goal of reproducible high cell performance has still not been reached. Improved cell mechanical tolerances and/or refinement of tile/electrode pore matching are indicated.

Electrolyte Development

The "conventional" high temperature tile powder synthesis has been discontinued in favor of the "aqueous slurry" method; tiles prepared from the latter process powder gave improved slump characteristics. Process development of the chloride synthesis for $LiAlO_2$ also continued, with emphasis on particle de-agglomeration. Porosity characteristics of $LiAlO_2$ "blanks" were compared with electrode porosity as an aid in explaining electrode flooding. B.E.T. surface area data for $LiAlO_2$ powders reveal a continuous decrease in surface area with time of cell operation, regardless of the initial surface area.

Electrode Studies

An anode sintering experiment, which included nickel, Nichrome alloy, and 316 stainless steel, was completed after 4000 hours. The results quantify the tendency of nickel anodes to sinter in an anode environment, and show the markedly improved sintering resistance of nichrome. A second sintering experiment, using improved cell environment simulation, is now underway.

Cell Tolerance to H_2S and HCl

Efforts to study the electrochemical efforts of non-sulfidizing concentrations of H_2S at the cell anode are being hampered by sulfidation of stainless steel inlet tubes at temperatures below cell operating temperatures. Alternative alumina cell designs are now being tested to avoid the presence of stainless steel. New cell studies with 100 ppm HCl added to both fuel and oxidant streams reveal an immediate and large performance decrease upon introduction of HCl. Post-mortem cell analyses reveal severe cathode compartment corrosion resulting from HCl.

Development of Scaled-Up Cells

Design of a 10" x 10" single cell has been completed and fabrication of all components is underway. The cell with incorporate the feature of independent pressurization of active area and seal area. Several changes were made in the earlier design, including an increase in current collector groove width and a decrease in groove depth to facilitate machining. In addition, initial studies (e.g., configuration and flow field design) leading to a 10" x 10" stackable sheet metal cell design were made.

INTRODUCTION

This report summarizes technical progress by the General Electric Company in the development of molten carbonate fuel cells for power generation. The described work covers the three month period between 15 November 1978 through 15 February 1979, and is funded by the Department of Energy under Contract EC-77-C-03-1479. Effort is organized into six tasks.

Task 1: System Definition and Integration

This task provides the information necessary to design appropriate experiments and interpret experimental data. Key elements include definition of anode/cathode reactant/contaminant compositions and flows, and the identification of preferred integration modes for coal gasifier/cleanup/fuel cell systems.

Task 2: Parametric Cell Studies

This task involves the development of a mathematical fuel cell model, the design and construction of model-compatible cell configurations, the experimental evaluation of fuel cell performance parameters, and the interpretation of results based on the parametric model. An iterative approach to both modeling and performance testing is being used. An additional goal of this task is to reach state-of-the-art performance levels using simulated coal-derived fuels.

Task 3: Electrolyte Development

This task includes all research and development related to the preparation of electrolyte/tile compositions and methods of tile fabrication. The properties and performance of tiles will be evaluated and optimized.

Task 4: Electrode Studies

In this task, the performance of various electrode materials will be evaluated, and suitable electrode preparation and attachment techniques will be developed.

Task 5: Contaminant Tolerance

This task involves the testing of cells in the presence of contaminants, and the establishment of tolerance limits for the major anticipated contaminants.

Task 9: Development of Scaled Up Cells

The standard 3" x 3" cell hardware will be scaled up to 10" x 10" hardware under this task. Activities include the design, fabrication, and testing of the larger cells, larger cell components, and required supporting hardware, such as electrolyte tile molds, cell clamping devices, and cell heaters.

1. SYSTEM DEFINITION AND INTEGRATION

There were no activities under this task during this quarter.

2. PARAMETRIC CELL STUDIES

2.1 EXPERIMENTAL CELL OPERATION

2.1.1 Introduction and Summary

Eleven fuel cell performance tests were carried out during this period. The primary focus of the test program was on the achievement of state-of-the-art performance levels on a reproducible basis. Significant modifications were made to the standard cell "package"; in particular, a new electrode system was employed in conjunction with tiles prepared from aqueous slurry process powder. These modifications resulted in markedly different cell operating characteristics. Significant improvements were made in both the cell resistance and electrode flooding problems cited previously. However, the goal of reproducible high cell performance was still not reached. In most cases where additional electrolyte was not added to the tile/electrode interface, the opposite problem, insufficient wetting of electrodes, was observed. Indications now point to needed improvement in cell mechanical tolerances and/or additional refinement of tile/electrode porosity matching; the latter is treated in Section 3.

2.1.2 Experimental Procedure

All fuel cell performance test runs used the standard 3" x 3" cell design described in previous reports. Modifications to the standard design have been made, and those modifications have been evaluated as a parameter; Table 2.1 summarizes the design/component parameters for each of the eleven performance runs. Most cells have now been modified to eliminate the removable current collector, where contact resistance at the cathode interfaces was a negative factor. However, in several cases, the removable current collector feature in conjunction with 347 stainless steel shims allowed the use of electrodes of varied thickness.

A change-over was made during the period to 30 mil thick anodes and 15 mil thick cathodes as standard; in particular, the reduced cathode thickness is expected to lower the ohmic resistance of the cathode. The new electrodes also have a somewhat different porosity characteristic, designed to mate with electrolyte tiles prepared by the aqueous slurry process.

No further changes were made during this period to standard operating procedures, such as fuel/oxidant compositions, mode of flow (counter-current), etc.

Table 2.1

Experimental Parameters

Run No.	Current Collector	Tile	Tile Process	Electrolyte Added	Electrode Thickness	Shims
CRD-039	Brazed	MSLA-95.C.28A	Chloride Impregnation	None	50 mil, Anode* 50 mil, Cathode*	No
CRD-041	Brazed	T-133	Chloride	None	50 mil, Anode* 30 mil, Cathode*	No
CRD-044	Removable	T-141M	Aqueous Slurry	None	50 mil, Anode* 20 mil, Cathode*	Yes
CRD-045	Integral	T-141M	Aqueous Slurry	None	30 mil, Anode** 15 mil, Cathode*	No
CRD-048	Removable	T-146M	Aqueous Slurry	0.2g/Surface	30 mil, Anode** 15 mil, Cathode*	Yes
CRD-050	Integral	HPE 256	Aqueous Slurry	None	30 mil, Anode** 15 mil, Cathode*	No
CRD-054	Integral	T-146M	Aqueous Slurry	None	30 mil, Anode** 15 mil, Cathode*	No
DECP-011	Integral	T-136M	Aqueous Slurry	0.25g/Anode	20 mil, Anode* 20 mil, Cathode*	No
DECP-012	Integral	T-137M	Aqueous Slurry	0.25g/Anode	20 mil, Anode* 20 mil, Cathode*	No
DECP-013	Integral	T-140M	Aqueous Slurry	None	20 mil, Anode* 20 mil, Cathode*	No
DECP-014	Integral	T-140M	Aqueous Slurry	None	20 mil, Anode* 20 mil, Cathode*	No

*Nickel
**Nickel Plus 10% Chromium

Because of the increased emphasis on cell testing, an additional test stand for 3" x 3" cells was constructed and became operational during this period.

2.1.3 Results and Discussion

Table 2.2 summarizes the purpose of each of eleven runs carried out during this period. In addition, Run CRD-027, the thermal cycle test run, was completed during this period; twenty-one thermal cycles were completed during 2424 hours of operation.

Cell Performance

Cell CRD-039 was assembled using brazed-in-place current collector inserts and a 50% electrolyte impregnation process electrolyte tile in order to decrease cell resistance and reduce flooding, respectively. Cell performance, however, was poor. Upon disassembly, it was observed that the tile had extruded out of the wet seal; a similar tile slumped badly in a separate out-of-cell experiment. It was concluded that poor electrolyte retention led to electrode flooding and poor performance, even with the lower electrolyte content tile. Figure 2.1 shows a polarization curve for Run CRD-039 at constant utilization (75% anode gas, 25% cathode gas), along with polarization curves for Runs CRD 041 and CRD-050.

Run CRD-041 used a thinner cathode (30 mil vs. 50 mil in Run CRD-039), the same brazed-in-place current collector inserts, and a 50% electrolyte/chloride process $LiAlO_2$ hot-pressed tile in another attempt to decrease cell resistance and minimize flooding. Performance was substantially improved, as shown in Figure 2.1, to a level comparable with some of the better performance runs reported previously (but not up to the desired levels, such as Run DECP-010). The performance improvement is attributed primarily to a better tile and lower (33mΩ) cell resistance. The lower cell resistance is likely related to the thinner cathode.

Runs DECP-011 through DECP-014 and Runs CRD-044, -045, and -048 were primarily devoted to the testing of tiles prepared by the aqueous slurry process. As a class, these tiles tend to be extremely "dry", and show little tendency to slump or yield. Sealing tends to be more difficult, and requires longer times to be established. In addition, cell performance tends to require a relatively long period of time (100-200 hours) to reach a steady level when compared with the typical 24 hour "start-up" times for tiles prepared by the "state-of-the-art" process. The first such run, DECP-011, exhibited very low cell resistance (12.4mΩ

Table 2.2

Purpose of Runs

Run No.	Purpose
CRD-039	Anode current collector plate was brazed in place with Cu/Au alloy to decrease the possibility of contact resistance. The tile, MSLA-95.C.28A, contained only 50% electrolyte.
CRD-041	The tile, T-133, contained only 50% electrolyte. The cathode was 30 mil thick to reduce the cell resistance.
CRD-044	Test of tile T-141M produced from aqueous slurry process powder. Additional electrolyte was not added.
CRD-045	Test of tile T-141M in modified hardware with new electrode system.
CRD-048	Repeat of previous run with addition of 0.2g.
CRD-050	Test of tile HPE 256 supplied by IGT.
CRD-054	Test of tile T-146M in hardware with improved alignment of cell components.
DECP-011	Performance test with first slurry process tile, T-136M.
DECP-012	Repeat of previous run with lower electrolyte content tile (58%).
DECP-013	Repeat of previous run with no added electrolyte.
DECP-014	Repeat of previous run.

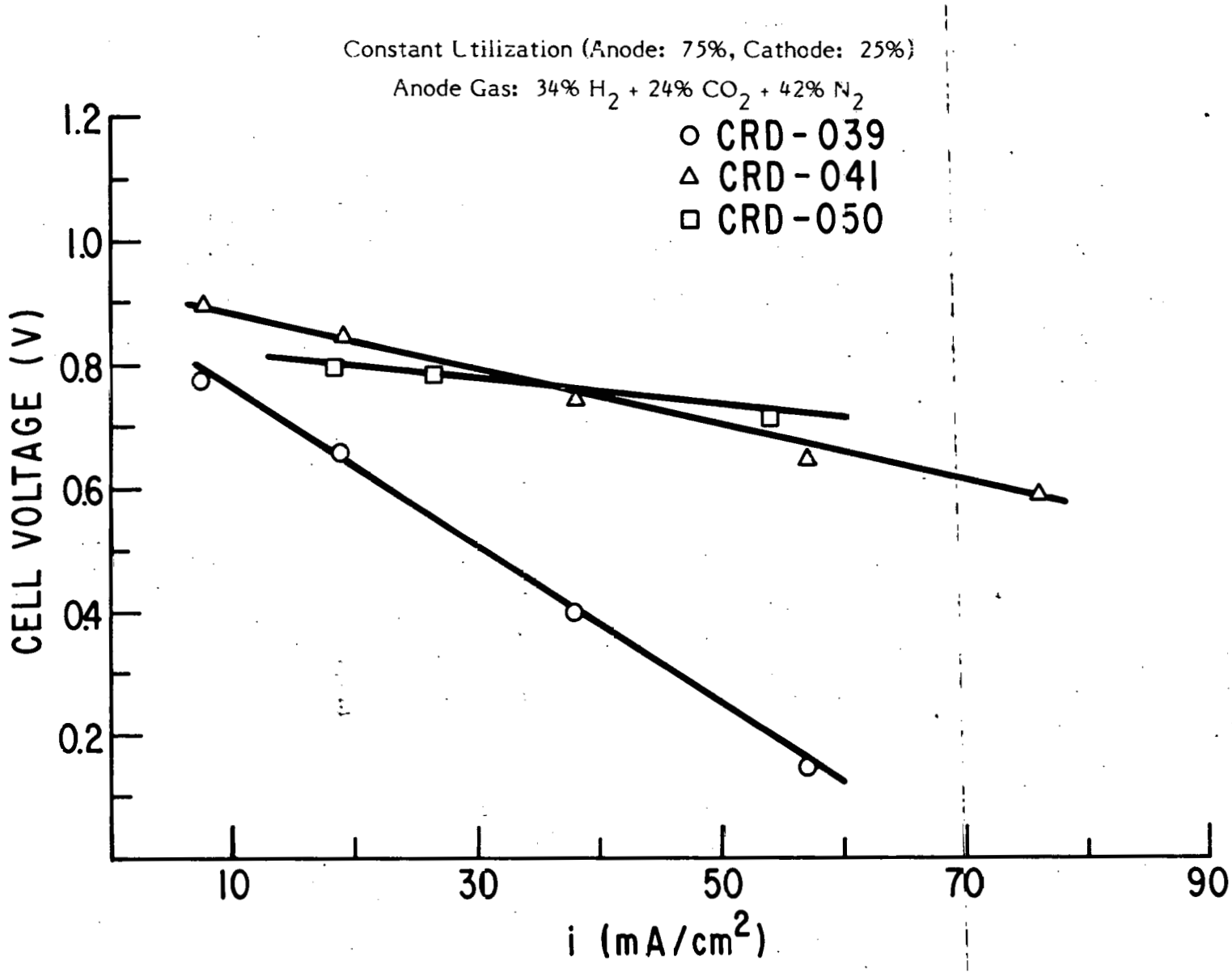

Fig. 2.1

Constant Utilization Polarization Curve For Runs CRD-039, CRD-041, and CRD-050

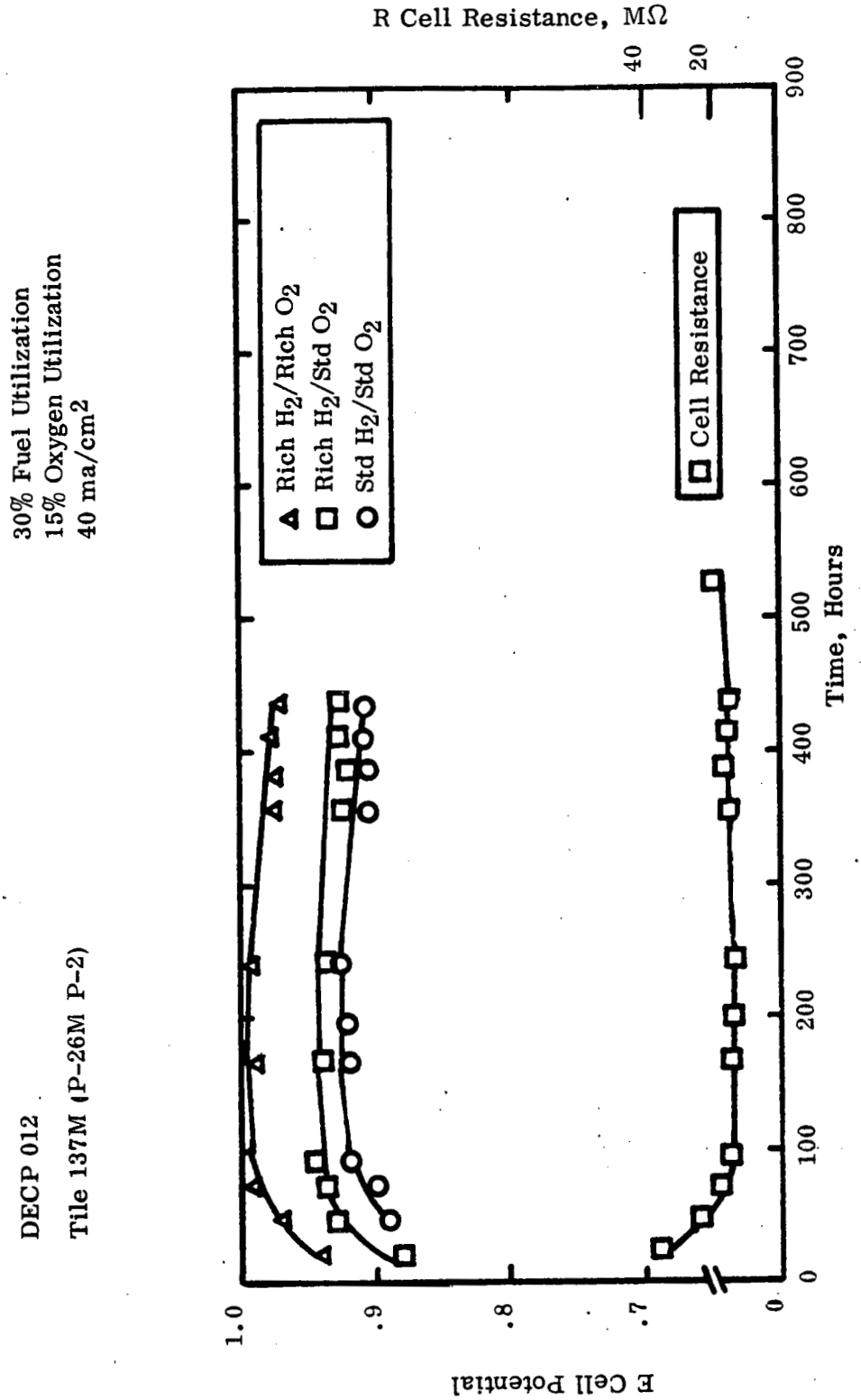

Fig. 2.2

Performance as a Function of Time For Run DECP-012

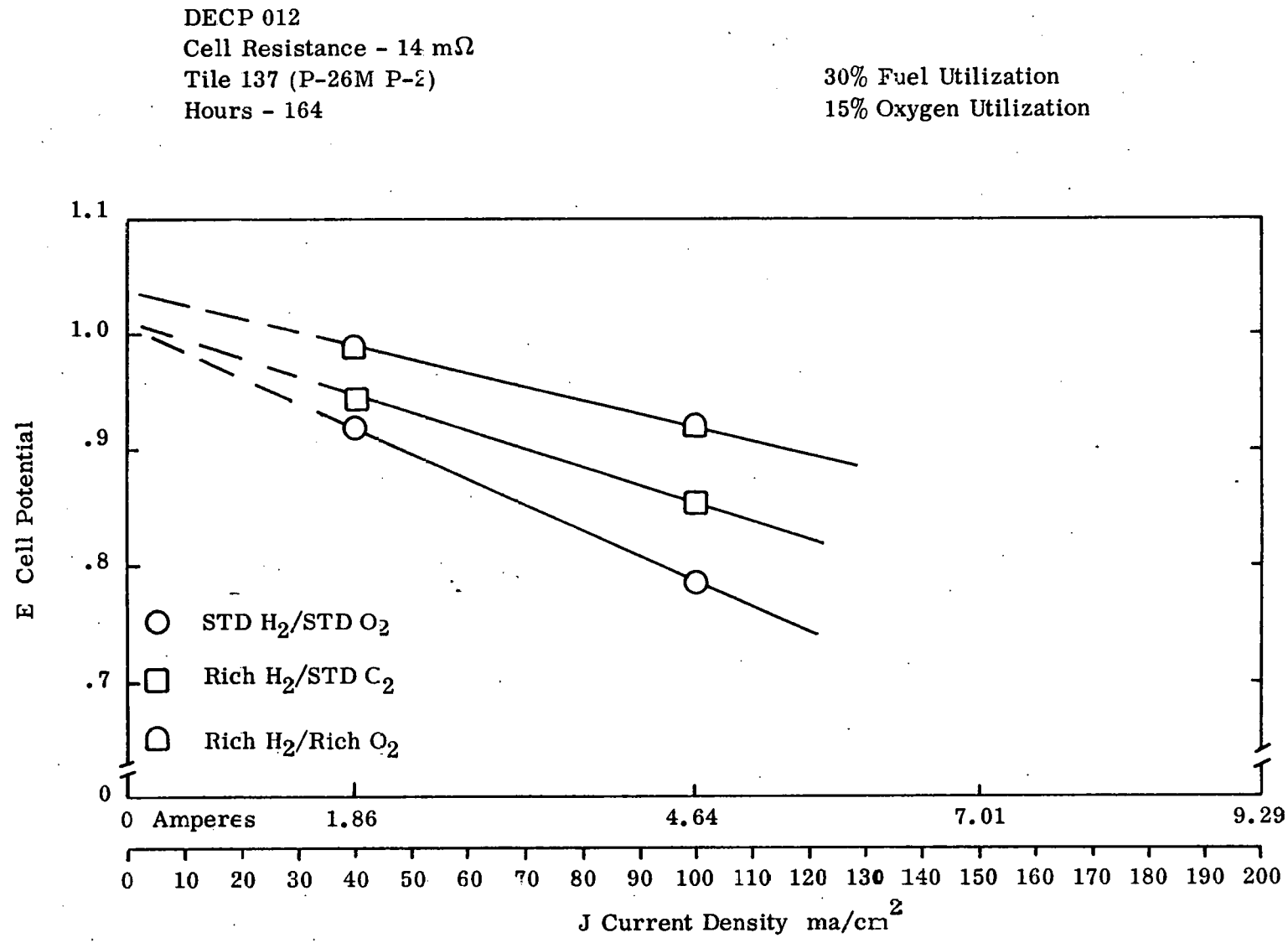

Fig. 2.3
Constant Utilization Polarization Curve For Run DECP-012

by the AC method at 1000 Hz) but very poor performance. The poor performance was traced to an error in tile manufacture which resulted in a 70% carbonate content tile.

A repeat of Run DECP-011, Run DECP-012, used a tile with 58% electrolyte, along with 0.25 g electrolyte added to each tile/electrode face. Figures 2.2 and 2.3 show performance with time and constant utilization polarization curves, respectively, for Run DECP-012. The 1000 Hz cell resistance decreased from 48mΩ on Day 1 to 24mΩ on Day 3 to 14mΩ on Day 5; little additional decrease was observed beyond Day 5. Likewise, two days were required before satisfactory wet-seals were established. During the five-day "start-up" period, performance steadily improved, as expected. During this period, the anode (pure nickel) showed an unusual sensitivity to fuel composition (more typically seen for cathodes) suggesting that either the anode was slow to wet or, the opposite, was flooding. Performance reached a relatively respectable level after 120 hours, as seen in Figure 2.3; performance leveled off and then began to decrease between 240 and 450 hours of operation, presumably due to sintering of the pure nickel anode. Cell performance was 0.79V at 100 mA/cm^2 with 30% standard fuel and 15% standard oxidant utilization. At 523 hours, a heater malfunction caused the cell to reach 724^{o}C and the cell was shut down.

On the theory that the Run DECP-012 anode may have been flooded, no electrolyte was added to the electrode/electrolyte interface in Run DECP-013. Operational difficulties were encountered; however, cell resistance was high, sealing was poor, and a cross-leak was present. Post-run observation revealed poorly wetted electrodes. Although sealing improved in Run DECP-013, cell resistance was very high (50mΩ), and performance was corespondingly poor. After 233 hours of operation, a cross-leak occurred and the cell was shut down. Again there was evidence of poor electrode wetting.

Run CRD-044 was a similar test of the aqueous slurry tile; again, sealing was poor and there was a small cross-leak. Performance was poor. Post-run analysis revealed poor electrode wetting.

Runs CRD-045 and CRD-048 were the first to use a new electrode system (see Section 4). Anodes were 30 mil thick nickel/chromium and cathodes were 15 mil thick nickel, obtained from Gould. Cell CRD-045 exhibited no improvement over the previous run, and, indeed, similar post-run observations were made. In order to offset the extreme "dryness", 0.2 g electrolyte/interface was added in Run

CRD-048. While seal and cross-leakage characteristics did improve, cell performance did not.

Run CRD-050 used a tile obtained from IGT. The tile was prepared by the aqueous slurry process and contained 56% electrolyte. Although seal leakage was high at the anode, and some cross-leakae occurred, performance, as shown in Figure 2.1, was comparable to Run CRD-041. An interesting feature of the polarization curve is the lower slope, indicating lower polarization for Run CRD-050; cell resistance, at 32mΩ, was comparable to Run CRD-041 (33mΩ). Disassembly of the cell, after declining anode and seal characteristics, revealed that the anode had "swelled" by 2 mils. The tile was removed intact, and there was evidence that non-uniform swelling of the anode led to only partial contact between anode and tile. There was similar evidence of only partial cathode contact as well. It was estimated that at least one-third of the tile was not in contact with the electrodes.

Evidence from the preceding runs suggest that poor electrode wetting may be the present performance limitation. Although electrode/electrolyte pore matching may be at fault, it is also possible that improved mechanical assembly is needed. Clearly, "dry" tiles are less forgiving than "wet" tiles in terms of mechanical assembly. Cell CRD-054 was assembled, therefore, with line-to-line alignment (with $\pm$.001") of the electrodes with the wet-seal face. Good sealing was achieved, and the initial performance of the cell was good. Figure 2.4 shows an initial constant-flow current-voltage curve for cell CRD-054, obtained after the second day of cell operation. Also shown are the results of reference electrode measurements, using the $Au/O_2/CO_2$ reference; the reference is located on the anode side so that the cathode to reference voltage includes the voltage drop in the tile. Note the high, but typical, losses at the cathode, and the contrasting small polarization of the anode. Cell CRD-054 is still on test and continues to improve.

If indeed mechanical asembly is shown to be a cause of performance losses, it would appear to be a seriously negative indication for stack functionality, since cell misalignment errors would be additive. With cells of the present design, tolerances to $\pm$.001" appear to be closest possible.

Cell Impedance Measurements

AC measurements of cell impedance were carried out as a function of frequency between 3 Hz and 10,000 Hz for several runs. The results for Run CRD-039 are shown in Figure 2.5. Values at frequencies below 30 Hz are not

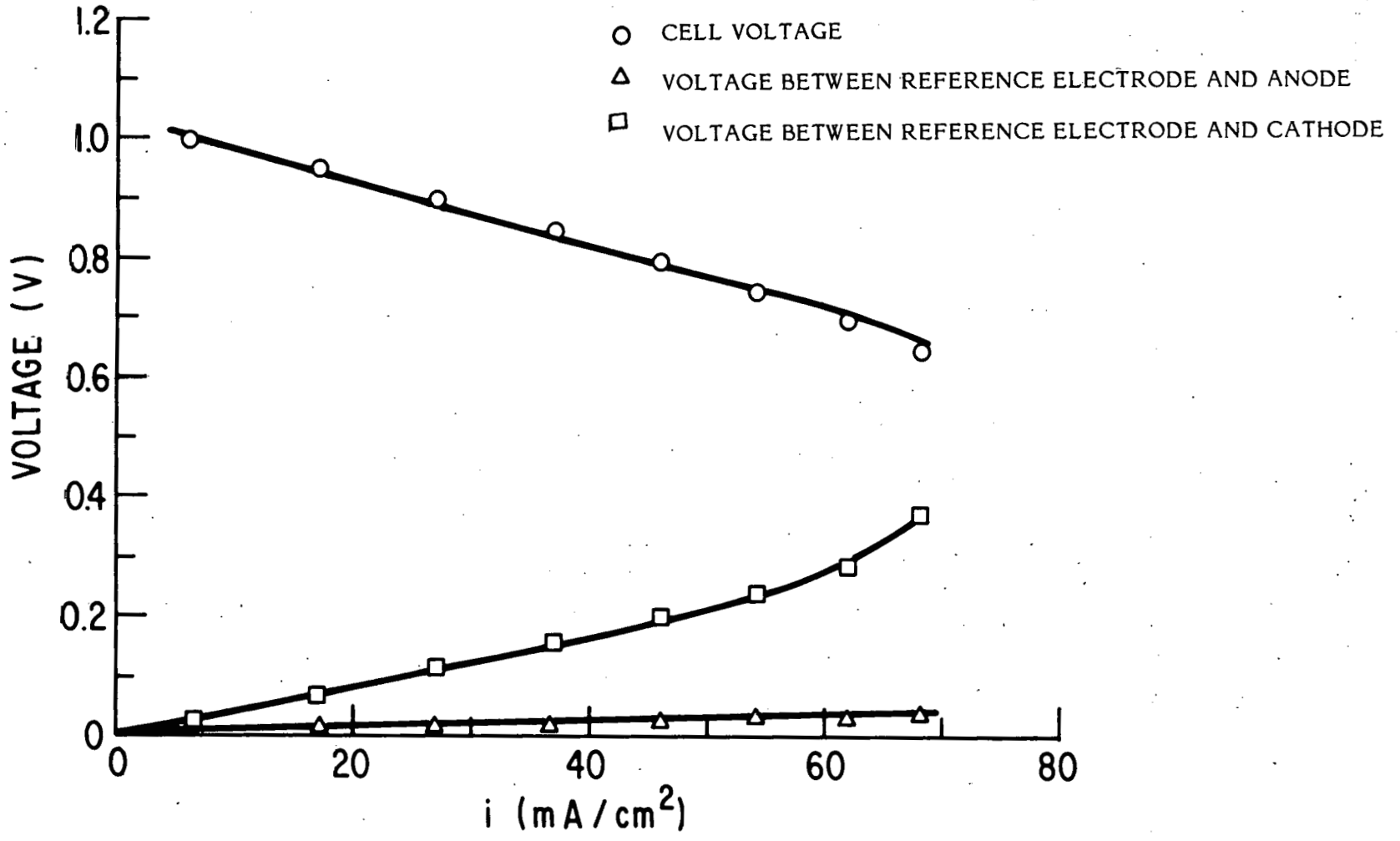

Fig. 2.4
Polarization Curves For Run CRD-054

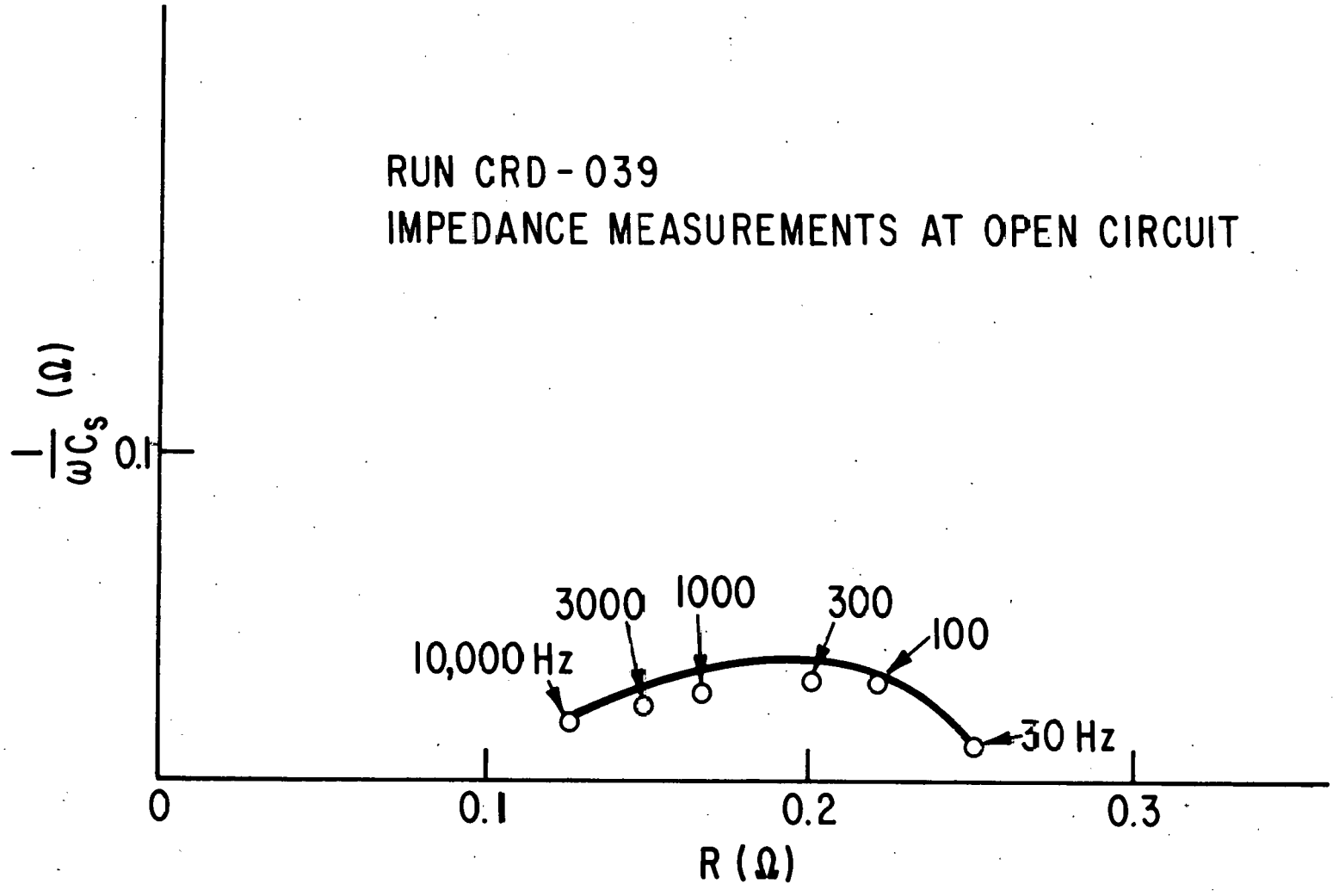
RUN CRD-039
IMPEDANCE MEASUREMENTS AT OPEN CIRCUIT
$-\frac{1}{\omega C_s}$ (Ω)
0.1
10,000 Hz
3000
1000
300
100
30 Hz
0
0.1
0.2
0.3
R (Ω)

Fig. 2.5

shown because both the absolute value of the impedance and the phase angle change slowly with time. This behavior indicates that dynamic processes, involving the motion of electrolyte and gases, occur in a periodic fashion inside the active region of the electrode. The plot of capacitive component versus ohmic component of the impedance in an analog series circuit of capacity and resistor cannot be approximated by a semicircle as it should be in the ideal case for an impedance of the said type with elements independent of frequency. In general, the capacitive component is considerably smaller than the ohmic component. A satisfactory interpretation of the results in Fig. 2.5 has not been developed. However, it appears feasible that measurements of this type could supply information concerning active regions inside the porous electrodes.

Cell Leakage Measurements

Table 2.3 summarizes the results of seal and cross-leakage for selected runs. The extent of leakage appears to be a function of tile "dryness" and of cell alignment. Wet seal leakage was low in the "wet" tile runs (CRD-039 and -041), and in the "dry" tile run where 0.2 g electrode was added (CRD-048), and seal leakage was moderate in the "dry" but closely aligned cell (CRD-0541). The remaining "dry" tile runs (CRD-044, -045, and -050) had unacceptably high seal-leakage rates (i.e., greater than 5%).

Similarly, cross-tile leakage closely paralleled the seal-leak observations. Cross-leakage is normally determined by an argon/mass spectrometer test, but, as indicated in Table 2.3, a measurement of open circuit potential under a given flow condition also provides a good measure of cross-leakage. Neither method gives a truly quantitive cross-leak measure, however, because of the variable seal-leaks from run to run. In general, an open circuit potential of 1.030V or above is indicative of the absence of a cross-leak.

2.1.4 Conclusions

Further understanding of cell performance has been gained, but the goal of reproducible high performance cells has not been reached. Through changes in both electrode and tile characteristics, substantially different cell characteristics were observed; with the apparent solution to the previously encountered flooding problems came the new problem of insufficient electrode wetting. An optimum electrode/tile combination lies between these two extremes.

Table 2.3

Results of Cell Leakage Measurements

Run No.	Leakage Wet Seal Anode	Leakage Wet Seal Cathode	Cross Leakage	Open Circuit Voltage At Gas Flow Of 100 cm^3/min
CRD-039	2%	2%	Not Detectable	1.035 V
CRD-041	2%	2%	Not Detectable	1.034
CRD-044	14%	14%	Small	1.023
CRD-045	9%	11%	Small	1.024
CRD-048	2%	3%	Not Detectable	1.032
CRD-050	20%	2%	Approximately 3%	1.010
CRD-054	3%	5%	Not Detectable	1.030

2.2 ANALYTICAL FUEL CELL MODEL

This subtask was inactive during this period.

3. ELECTROLYTE DEVELOPMENT

3.1 SUMMARY

The "conventional" high temperature synthesis method for producing electrolyte tile powders has failed to yield electrolyte tiles with reproducible properties, in spite of continued process development. That method has, at least temporarily, been discontinued in favor of the "aqueous slurry" method. The latter method was used to produce powders which resulted in tiles with excellent "slump" characteristics.

Increased emphasis has been placed on tile diagnostics. Analytical data, collected for a variety of tile samples before and after use in an operating cell, reveal a continuous decrease in $LiAlO_2$ surface area with operating time. Porosimetry data on electrodes and chloride synthesis $LiAlO_2$ blanks (precursors to impregnation tiles) indicate the presence of agglomerates, which lead to a broad pore distribution in the tile and excessive porosity overlap with the electrodes. By additional wet-milling of the $LiAlO_2$, the tile blank porosity characteristics was sharpened and pore overlap with the electrodes was reduced.

3.2 TILE COMPOSITION SYNTHESIS

3.2.1 Powder Batch Development

Despite a continuing development effort, the "conventional" powder batch synthesis (i.e., the stepwise reaction of gamma-Al_2O_3 with Li_2CO_3 in the presence of a K_2CO_3-rich melt) has failed to yield a powder which can be fabricated into the tiles with reproducibly good properties. In general, tiles prepared from "conventional" synthesis powder tended to have poor slump characteristics (i.e., very wet). As a result, further development of this process has been discontinued for the present.

This process is being replaced by the aqueous slurry process for the preparation of "standard" powders for "standard" tiles; development of the chloride process for $LiAlO_2$ synthesis is also continuing (see below).

The procedure for the aqueous slurry process is the same as that outlined in a recent IGT report (3.1). It involves the preparation of a $LiOH{\cdot}H_2O$ plus gamma-Al_2O_3 aqueous slurry, followed by drying at 110°C, carbonation, and K_2CO_3 addition. Four 2500 g powder batches were prepared by the procedure during this

quarter. Table 3.1 contains analytical data for the four batches. Batch P-26M was divided into to smaller batches part way through processing for convenience of handling. Before dividing the batch, the slurry was inadvertently dried at 140°C (versus 110°C desired) due to an oven malfunction. A processing error with batch P-26M (P-1) resulted in an unacceptably high (70%) carbonate content powder. Adjustments to batch P-26M (P-2) resulted in the proper carbonate content. Batches P-26M and P-27M could be pressed into tiles which showed good results in the 650°C/CO_2 slump test; batch P-28M has not been evaluated.

3.2.2 Electrolyte-Free $LiAlO_2$ Preparation

The quarter's effort was directed toward the preparation of smaller crystallite size $LiAlO_2$ than that prepared in the previously reported (3.2) "chloride" synthesis. It is generally recognized that a smaller crystallite sized material should give improved electrolyte retention characteristics, provided it is stable against crystal growth. This effort was based on a low temperature "chloride" synthesis using a solvent composed of 54 mole% LiCl-9 mole% NaCl-37 mole% KCl. This solvent reportedly has a liquidus temperature of ~623K, although experiments in this laboratory indicate the liquidus of the combined chloride-LiOH system lies in the range 643-673K.

Experiments to date have been only partially successful in that although a predominantly β-$LiAlO_2$ produce was prepared, it was contaminated with a phase which was difficult to characterize by x-rays. Based on previous work (3.2), this phase is most likely unreacted, poorly crystallized γ-Al_2O_3. This conclusion is reinforced by the sample's surface area of $\geq$ 30 $meter^2 gram^{-1}$. Modifications to the synthesis are being explored which will promote reaction at these low temperatures while preserving the desired small crystallite size.

3.3 ELECTROLYTE TILE FABRICATION

3.3.1 "Conventional" Hot-Pressing Fabrication

A total of 21 tiles were fabricated during this quarter. Table 3.2 is a summary of the characteristics of tiles T-131A through T-151M. Four of these tiles (T-131A through T-134A) were fabricated using "chloride" process electrolyte powder. The remaining seventeen tiles were made using "aqueous slurry" process electrolyte powder. Tiles 135M and 136M were made with powder P-26MP1 which inadvertently had a high carbonate content (70 wt %). Even at this high carbonate

Table 3.1

Characterization of New Powder Batches

Powder Batch	Wet Analysis $LiAlO_2$ Wt %	Wet Analysis Carbonate Wt %	B.E.T. Surface Area M^2/g	X-Ray Allotropic Form α	β	γ
P-26MP1	30	48	33.9	92	8	0
P-26MP2	42	58	27	67	29	4
P-27M	40	60	21.6	31	69	0
P-28M	48	52	Not Available Yet			

Table 3.2

Log of Tiles Pressed

Tile Sample Number	Tile Comp. Number	Die Size cm	Pressure kg/cm^2	Pressing Temp. ^oC	Tile Thickness cm	Tile Density (g/cc)	Comments[1]
T-131A	P-24A	11.43	504	480°	.142	2.28	Chloride Process Batch A-1
T-132A	P-25A	11.43	504	480°	.160	2.35	Chloride Process Batch A-1
T-133A	P-25A	11.43	504	480°	.163	2.37	Chloride Process Batch A-1
T-134A	P-24A	11.43	504	480°	.155	2.24	Chloride Process Batch A-1
T-135M	P-26M P-1	11.43	504	480°	.142	2.32	
T-136M	P-26M P-1	26.67	497	480°	.246	2.44	
T-137M	P-26M P-2	11.43	504	480°	.114	2.31	
T-138M	P-27M	11.43	504	480°	.180	2.22	
T-139M	P-27M	11.43	504	480°	.170	2.31	
T-140M	P-26M P-2	26.67	497	480°	.152	2.43	Slight Crack
T-141M	P-27M	26.67	497	480°	.128	2.32	Cracked
T-142M	P-27M	26.67	497	480°	.157	2.32	Edges Cracked

Table 3.2 (Continued)

Log of Tiles Pressed

Tile Sample Number	Tile Comp. Number	Die Size cm	Pressure g/cm^2	Pressing Temp. ^{o}C	Tile Thickness cm	Tile Density (g/cc)	Comments
T-143M	P-27M	26.67	497	480°	.183	2.32	No Cracks
T-144M	P-27M	26.67	497	480°	.218	2.28	Kanthal Reinforced(2)
T-145M	P-27M	26.67	497	480°	.206	2.28	Kanthal Reinforced(2)
T-146M	P-27M	26.67	497	480°	.191	2.27	Kanthal Reinforced(2)
T-147M	P-26M P-2	26.67	497	480°	.179	2.36	Kanthal Reinforced(2)
T-148M	P-27M	26.67	497	480°	.180	2.32	No Cracks
T-149M	P-26M P-2	26.67	497	480°	.198	2.26	No Cracks
T-150M	P-26M P-2	26.67	497	480°	.152	2.44	One Small Corner Crack
T-151M	P-26M P-2	26.67	248	485°	.178	2.33	One Small Corner Crack

(1) All tiles used powder made by the "aqueous slurry method" except as noted.
(2) Two layers of Kanthal screen woven to 20 x 20 mesh with .005 inch diameter wire.

level, samples of the tile stood up well in the 650°C/CO_2 slump test. No rounding of edges was observed on these samples; however, some very small cracks were present. Samples of tiles made from batches P-26M (P-2) and P-27M showed no cracking, blisters or slumping after the 650°C, CO_2 slump test. These were by far the best slump test results to date.

During this reporting period, three 10.5" x 10.5" tiles (140M, 141M and 142M) were manufactured from powder batches P-26M (P-2) and P-27M. All three exhibited some degree of cracking during the fabrication process. Corrective action was taken to eliminate or minimize the cracking in unreinforced tiles. These measures included an increase in tile thickness to greater than .072 inch (.183 cm) and an increased deposit of graphite mold release agent on the plungers. Tiles T-143M, 148M and 149M were all fabricated without cracks or broken corners using these process changes. The improved tensile strength of the tile, resulting from the increased tile thickness, allowed the tile to shrink during the manufacturing cooling cycle without fracturing.

Four tiles (T-144M, 145M, 146M and 147M) were reinforced with two layers of Kanthal A-1 screen. The procedure to center the screens within the tile was as follows:

- Flatten the Kanthal screens.
- Spread 1/3 the powder charge within the mold cavity.
- Place one screen over the powder in the mold cavity.
- Spread 1/3 the powder charge over the first screen.
- place the second screen over the powder layer.
- Spread the final 1/3 layer of powder over the second screen.

All four reinforced tiles were manufactured without difficulty.

The final tile fabricated during this quarter (T-151M) were pressed at one-half the standard pressure (248 kg/cm^2 vs. 497 kg/cm^2) and at a slightly higher temperature (485°C vs. 480°C) than normally used. Its density was well within the variation of tile densities for a given powder batch.

3.3.2 Impregnation Tile Fabrication

There was no effort in this area during the past quarter due to the existence of both a sufficient quantity of such tiles and the results of the electrolyte tile diagnostic measurement contained below.

3.4 ELECTROLYTE TILE DIAGNOSTICS

Post-Run Tile Analysis

For selected runs, the tile material was carefully removed after the run and analyzed for chemical content ($LiAlO_2$ vs. carbonate), phase (x-ray), surface area (B.E.T.) and particle morphology (S.E.M.). Table 3.3 summarizes the analytical results. The cells chosen for analysis represent varied operating times and varied tile starting characteristics. The $LiAlO_2$ was retrieved from the used tiles by dissolution of the carbonate phase in an equal volume mixture of glacial acetic acid and acetic anhydride, followed by washing with absolute methanol and drying at $673^{o}K$ for several hours.

These data clearly indicate the decrease in surface area which all $LiAlO_2$ particles undergo, regardless of starting surface area. Further, there is no indication that the process is complete even after 2400 hours. Figure 3.1 graphically presents the surface area vs. time data. Although the data could be interpreted in various ways, the data could be separated into two distinct bands of similar slope: one band for the high starting surface area (27 and 33.9 m^2/g) and one for the lower starting surface area (6.4 to 11.4 m^2/g) $LiAlO_2$.

Table 3.3 also shows major changes in the phase analysis of $LiAlO_2$ for Cell DECP-010. The amount of β-$LiAlO_2$ in the seal area decreased by 68%, while alpha-$LiAlO_2$ increased by 100%. A corresponding change in the active area was not observed. In the only other cell for which data are now available (Cell DECP-011), no such change was observed, but the time of operation was relatively short (212 hours). More data are need to confirm any trend.

Several samples have been examined with the scanning electron microscope, representative data of which are contained in Figures 3.2, 3.3 and 3.4. These data reveal no striking differences between the three materials which would explain the relatively better electrochemical performance of cell DECP-010. The similarity in "used" matrix $LiAlO_2$ is more striking in view of the fact that the tile for CRD-027 was fabricated by the impregnation technique from "chloride" synthesis $LiAlO_2$. The remaining tiles were hot press fabricated from "conventionally" synthesized matrix-electrolyte mixtures, one synthesized at CRD (CRD-028), the other at DECP (DECP-010). The fuel cell operating conditions appear to erase the effects of the synthesis and processing histories from the matrix within a relatively short time. Additional data on used matrix characteristics will be added to this data base as it becomes available.

Table 3.3

Tile Diagnostics: Analytical Results

Sample	Hrs.	Wt. % $LiAlO_2$	Carbonate	Surface Area M^2/g	$LiAlO_2$ Allotropic Form α	β	γ
T-67 (P-13)	0	35	65	11.4	45	28	27
Cell DECP-010 (Active Area)	700	43	57	3.6	49	25	26
Cell DECP-010 (Seal Area)		46	54	2.8	40	8	52
T-136M (P-26M P1)	0	30	70	33.9	92	8	0
Cell DECP-011 (Active Area)	212	39	61	3.8	94	6	0
Cell DECP-011 (Seal Area)		39	61	8.3	96	4	0
T-137M (P-26M P2)	0	42	58	27	67	29	4
Cell DECP-012 (Active Area)	523	43	57	7.0	Not Available Yet		
Cell DECP-012 (Seal Area)		45	55	4.4	Not Available Yet		
T-140M (P-26M P2)	0	42	58	27	67	29	4
Cell DECP-013 (Active Area)	165	45	55	9.8	Not Available Yet		
Cell DECP-013 (Seal Area)		43	57	9.0	Not Available Yet		
T-140M (P-26M P2)	0	42	58	27	67	29	4
Cell DECP-014 (Active Area)	235	42	58	8.1			
Cell DECP-014 (Seal Area)		43	57	7.3			
MSLA-95-C-15B	0	45	55	6.4	11	72	17
CRD-027	2424	Not Available		2.4	Not Available Yet		
T-64 (Q-7)	0	40	60	9.1	Not Available Yet		
CRD-028	192	Not Available		3.8	Not Available Yet		

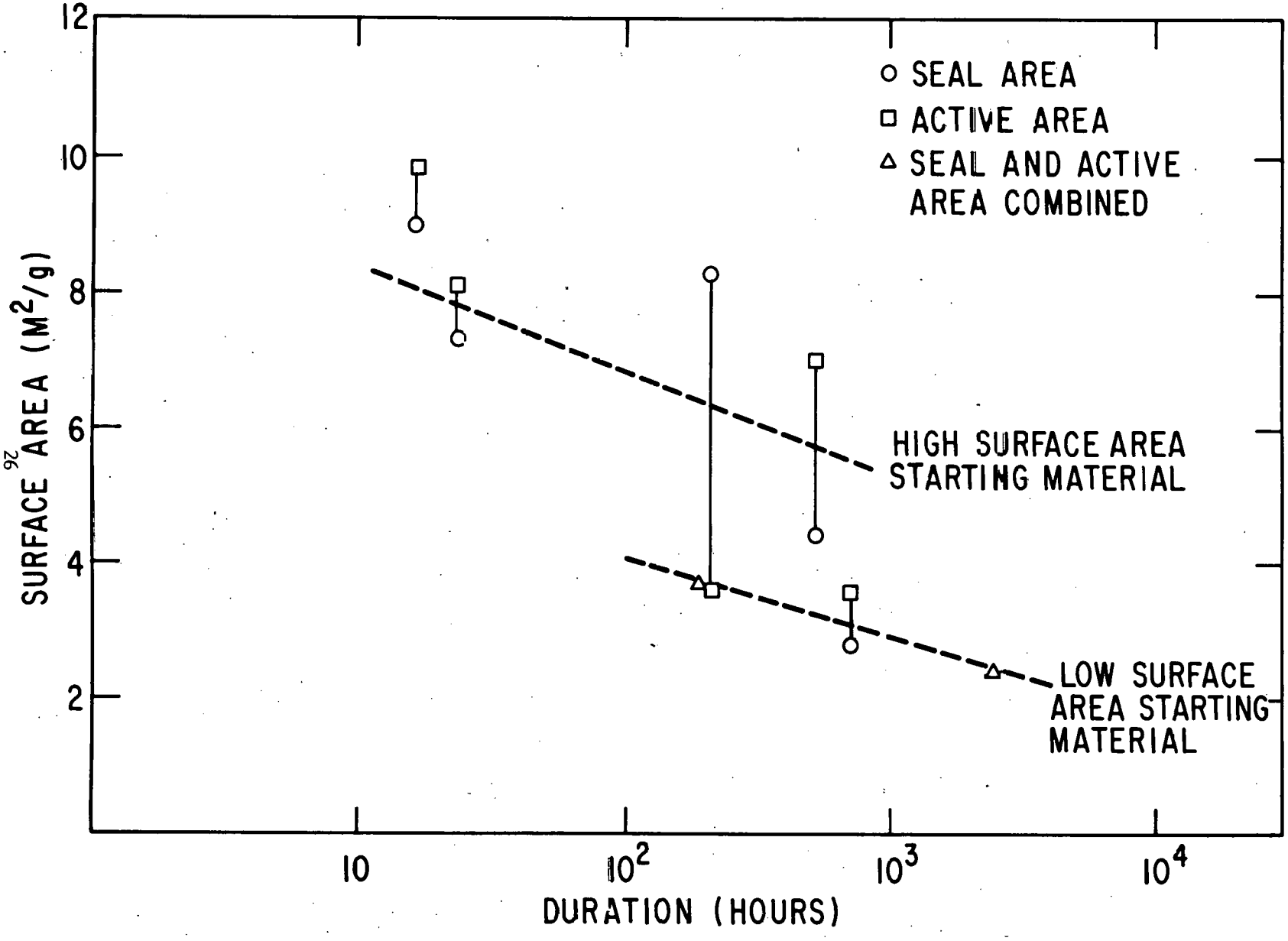

Fig. 3.1
$LiAlO_2$ B.E.T. Surface Area Changes With Time

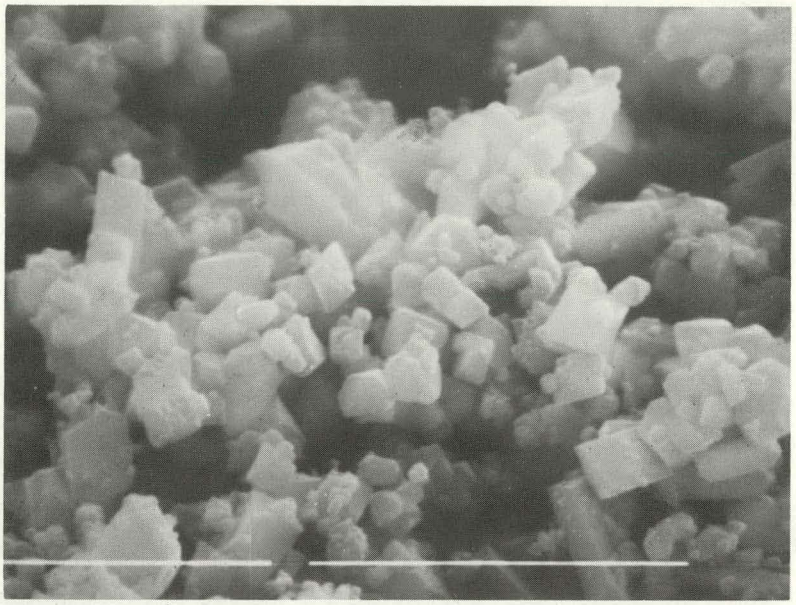

Figure 3.2: $LiAlO_2$ from CRD-028 (10,000 X).

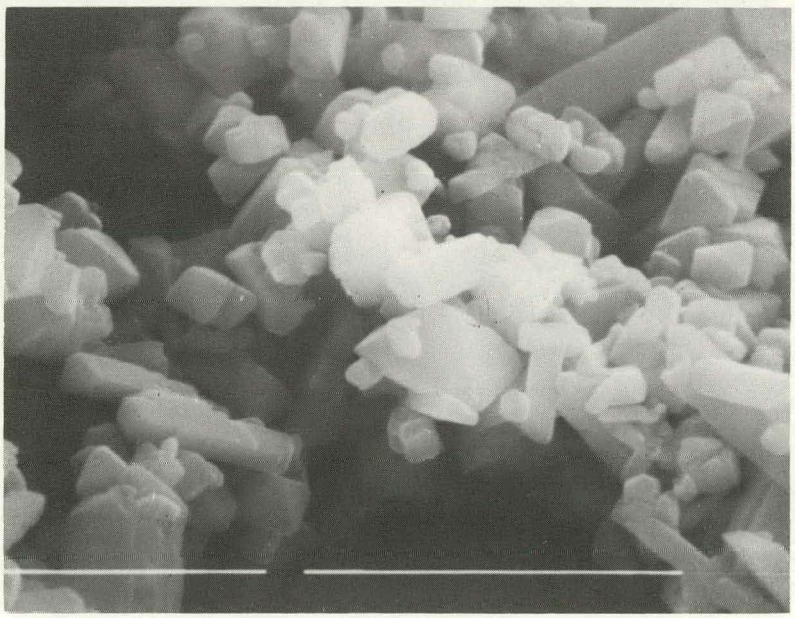

Figure 3.3: $LiAlO_2$ from DECP-010 (10,000 X).

Figure 3.4: $LiAlO_2$ from CRD-027 (10,000K).

Pore Matching

A study was conducted on materials and processes used in the "impregnation" preparation technique for the electrolyte structure, utilizing "chloride" synthesis $LiAlO_2$. The pore volume (fractional and accumulated) versus pore diameter data for $LiAlO_2$ matrix blanks prepared from different powder lots and at different cold-pressing pressures were compared with those data for both virgin and used electrode structures from cells operated during 1978. This comparison was not conducted on material from "conventionally" prepared electrolyte structures because it was felt that there was no justification in assuming that the matrix $LiAlO_2$ could be retrieved from its mixture with the carbonates, then reconstituted into a crystallite array that would resemble the configuration in the initial electrolyte structure. However, the conclusions reached in this study can equally well explain the failure of "conventionally" prepared electrolyte structures to perform properly.

The matrix $LiAlO_2$ samples were prepared by pressing $\sim$0.30 g of the as-prepared material in a 12.7 mm diameter steel die at the indicated pressure. The samples were either measured as-pressed, or they were given an ignition at $\sim$923K in an air atmosphere. It was found part way through the study that binder levels of $\leq$ 0.5 wt% did not alter the measurement perceptibly, therefore the ignition was omitted in later samples. The virgin electrode materials were measured in the as-received condition. Used electrode structures were retrieved from cell experiments by dissolution of the carbonate from the bonded electrode-electrolyte composite using an aqueous solution 2.0 molar in both acetic acid and sodium acetate. This solution was found to dissolve $\ll$0.1 wt% of either NiO or metallic Ni over a 24 hour period, but to completely dissolve the electrolyte. The freed electrodes were then copiously washed with distilled H_2O and, finally, absolute methanol before drying at $\sim$373K. The porosity measurements were made, as previously reported (3.2), using a Hg porosimeter.

Figures 3.5A,B contain the data for the material (MSLA-95 $LiAlO_2$) and conditions used in the preparation of the majority of impregnation fabricated tiles, including the tile used in experiment CRD-027. These data showed that a broad, poorly defined porosity distribution existed in matrix blanks pressed from as-prepared "chloride" synthesis $LiAlO_2$ at a cold pressing pressure of 13.79 MPa. A substantial fraction of the pore volume exists in pores with diameters $\geq$ 1.0 μm. Further, there is the indication of an additional peak in the distribution at pore diameters $\geq$10μm.

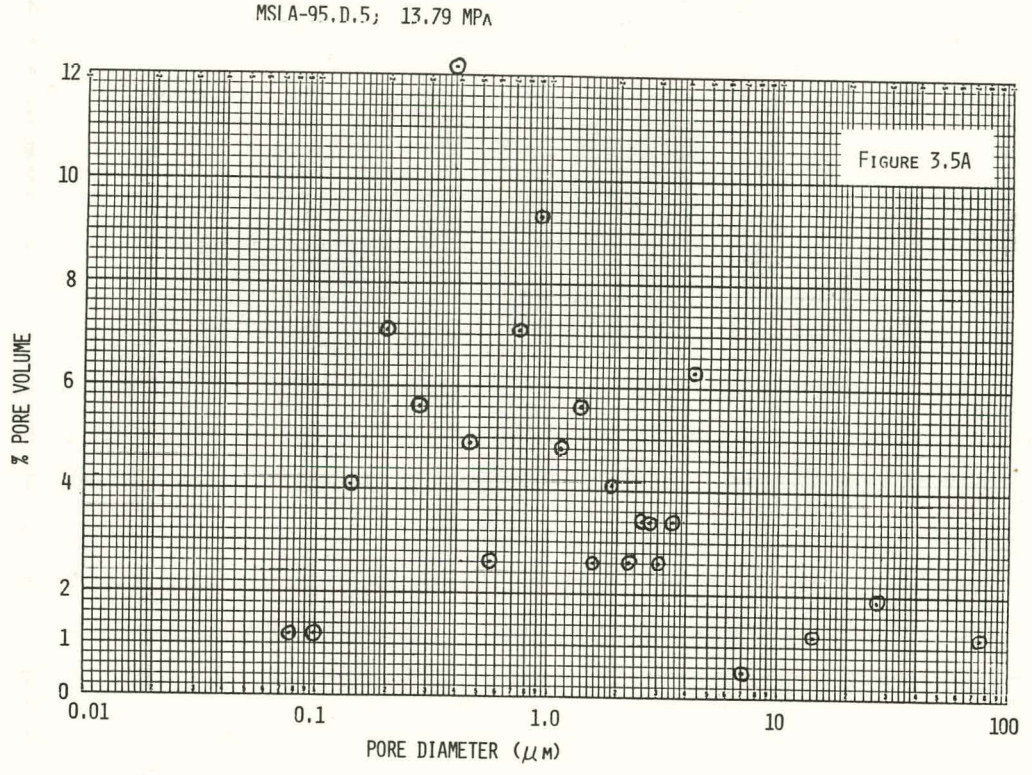

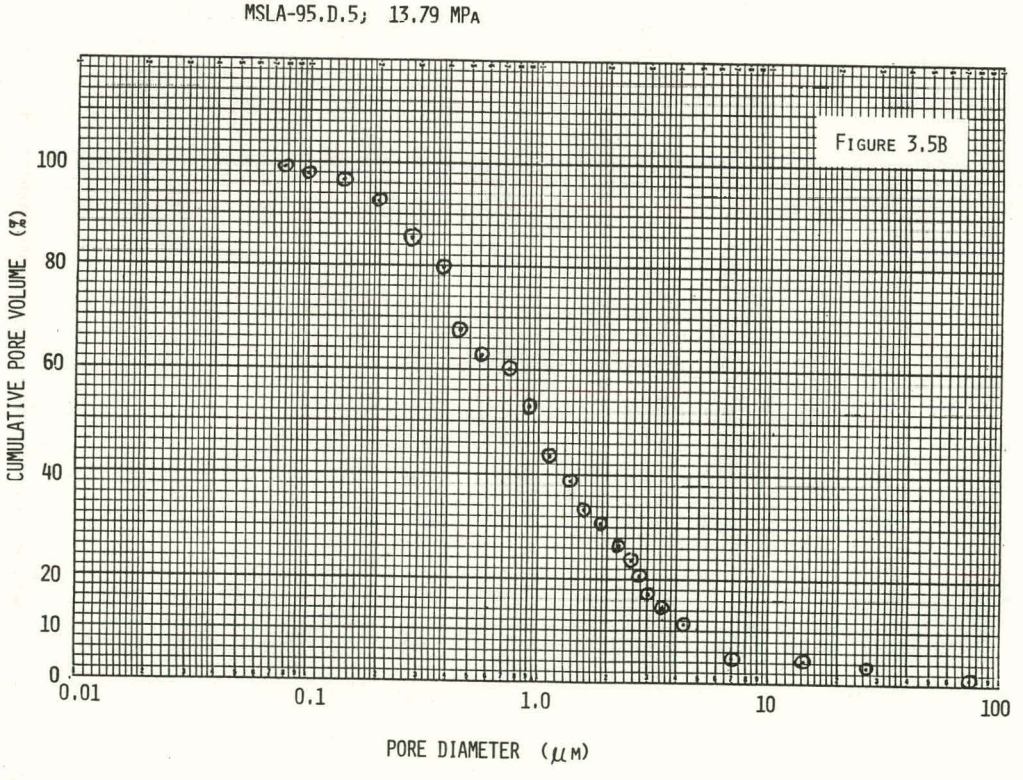

Fig. 3.5 A and B

Porosity Profile For $LiAlO_2$ Blank

Increasing the pressing pressure to 34.47 MPa, Figures 3.6A,B, resulted in some sharpening of the distribution relative to that in the 13.79 MPa pressing. However, there are still substantial volumes of porosity in large ($\geq$ 1.0μm) diameter pores, as well as an indication of a second peak at very large (>10μm) pore diameters. The improvement is not substantial.

A second lot of $LiAlO_2$ (MSLA-100) was examined in the same manner. This material had a B.E.T. surface area of 7.67 meters^2 gram^{-1}, compared with 6.43 meters^2 gram^{-1} for the previous material. One would therefore expect the smaller crystallite size of the second lot of material to manifest itself as an improved porosity distribution. Figures 3.7A,B show the data for a 34.47 MPa pressed sample of this material, which were equivalent to the data from a 13.79 MPa pressed sample. This distribution is poorer in terms of its definition and location than those shown in Figures 3.5 and 3.6, the opposite of the behavior anticipated from the surface area measurements. Based on these data, it was concluded that although the "chloride" synthesis yields a reasonably constant average crystallite size, as measured by B.E.T., the extent of agglomeration of these crystallites is not controlled and is apparently highly variable.

The materials represented by the data in Figures 3.5, 3.6 and 3.7 are unattractive when viewed in the context of those attributes held necessary for good electrolyte retention and cell performance. This conclusion is reinforced by a comparison with virgin and used electrode materials. Although the comparisons are made only for the material and conditions represented in Figure 3.5, they are valid for the other materials and conditions considered heretofore. Figures 3.8A,B compare the matrix with the virgin electrode material used in experiments CRD-027 and CRD-028. These data indicate that the initial porosity matching is reasonable, with porosity overlap being < 20%.

A comparison with the anode and cathode porosity data for experiment CRD-027 is shown in Figures 3.9A,B. The overlap has increased due to broadening of the anode and cathode porosity distributions relative to the virgin electrode material. The actual situation is likely to be far worse in that the crystal growth of the matrix $LiAlO_2$, which will act to increase the average pore diameter, has not been included in these comparisons. Figures 3.10A,B make the comparison with the anode and cathode from experiment DECP-010. The virgin electrode material for this experiment differed only slightly from that used in experiments CRD-027 and -028, although DECP-010 gave excellent electrochemical performance. It was

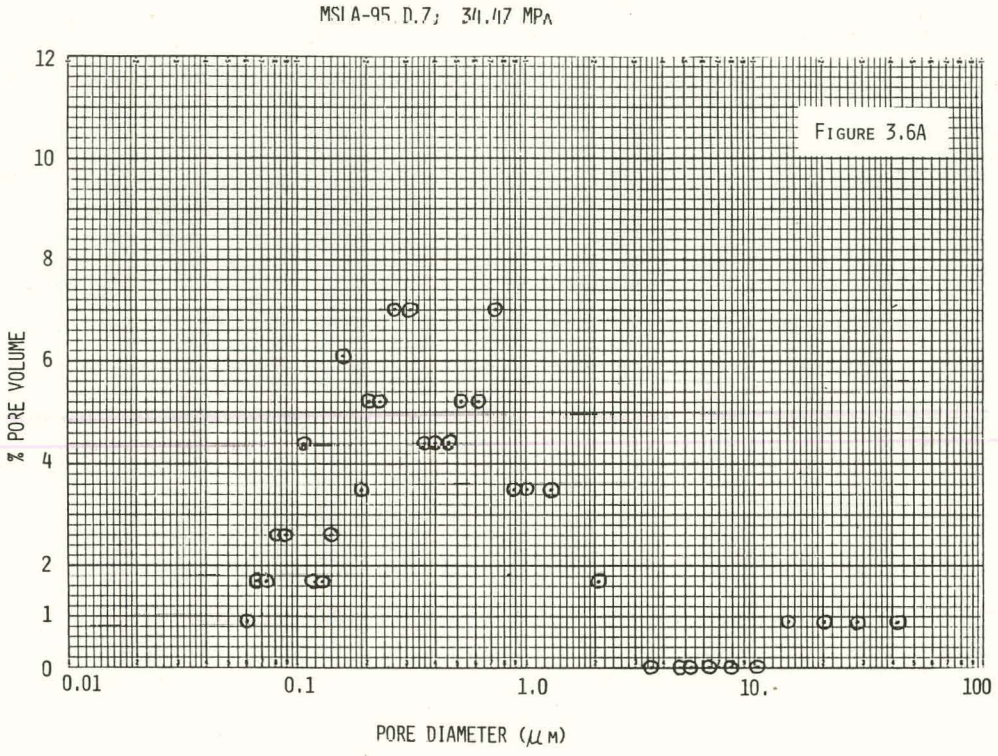

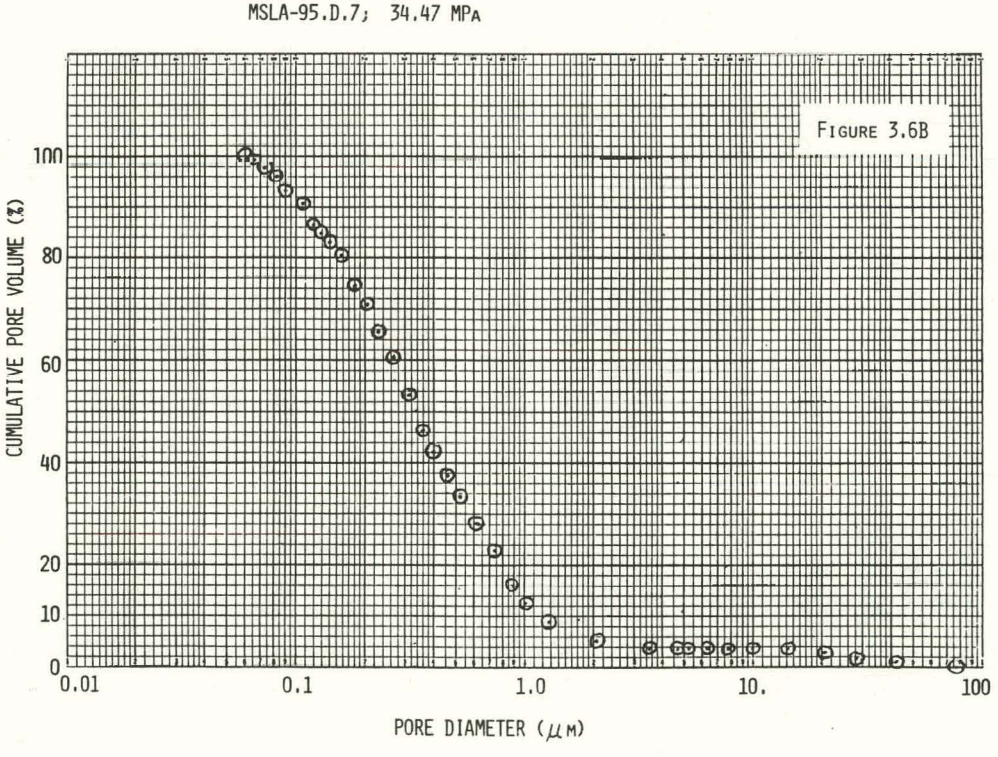

Fig. 3.6 A and B

Porosity Profile For $LiAlO_2$ Blank

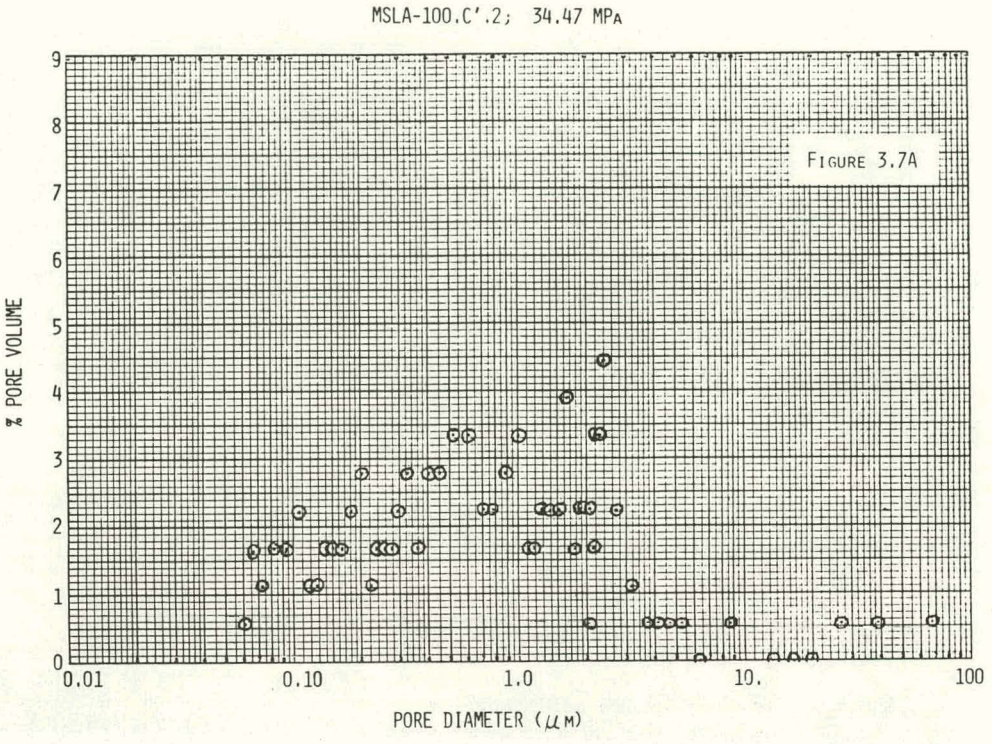

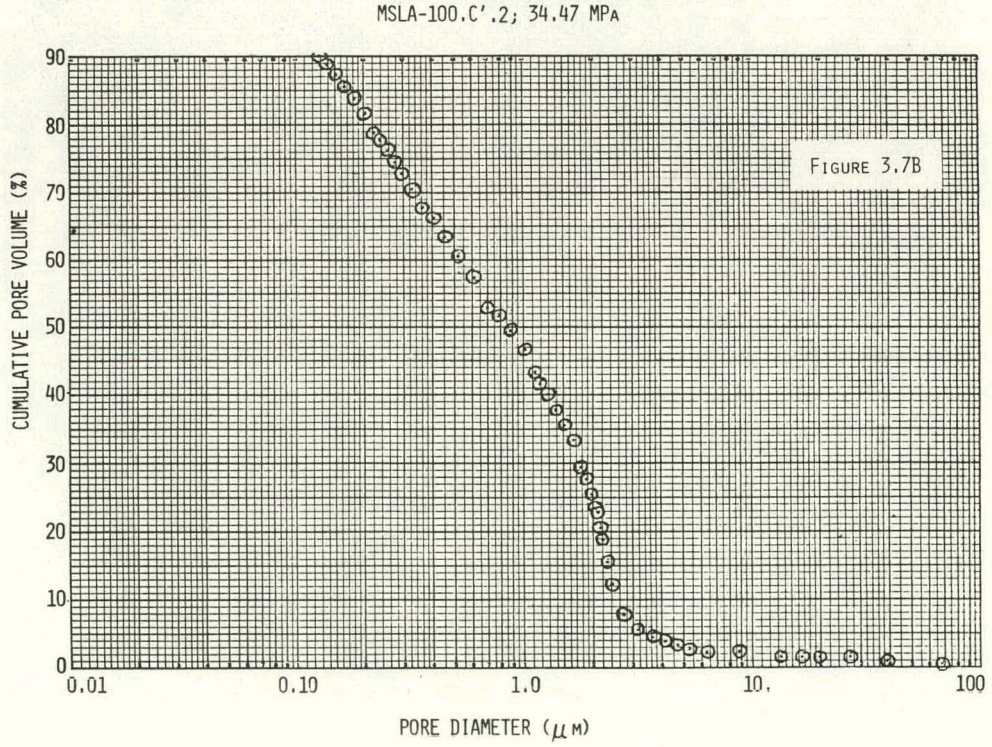

Fig. 3.7 A and B

Porosity Profile For $LiAlO_2$ Blank

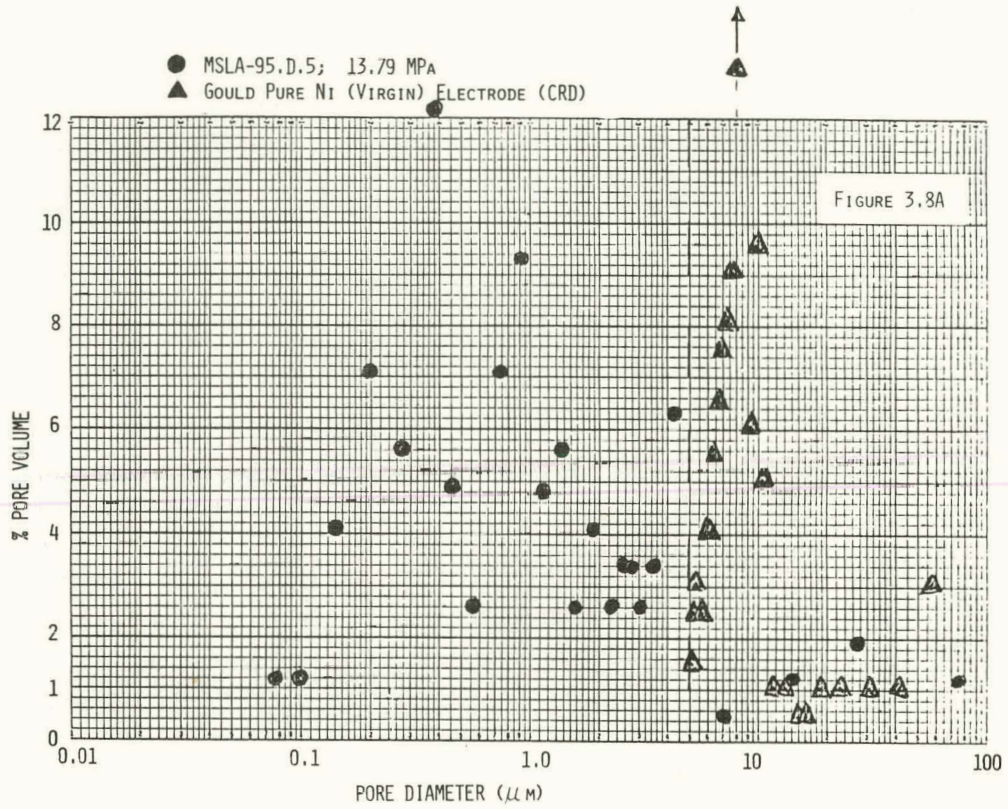

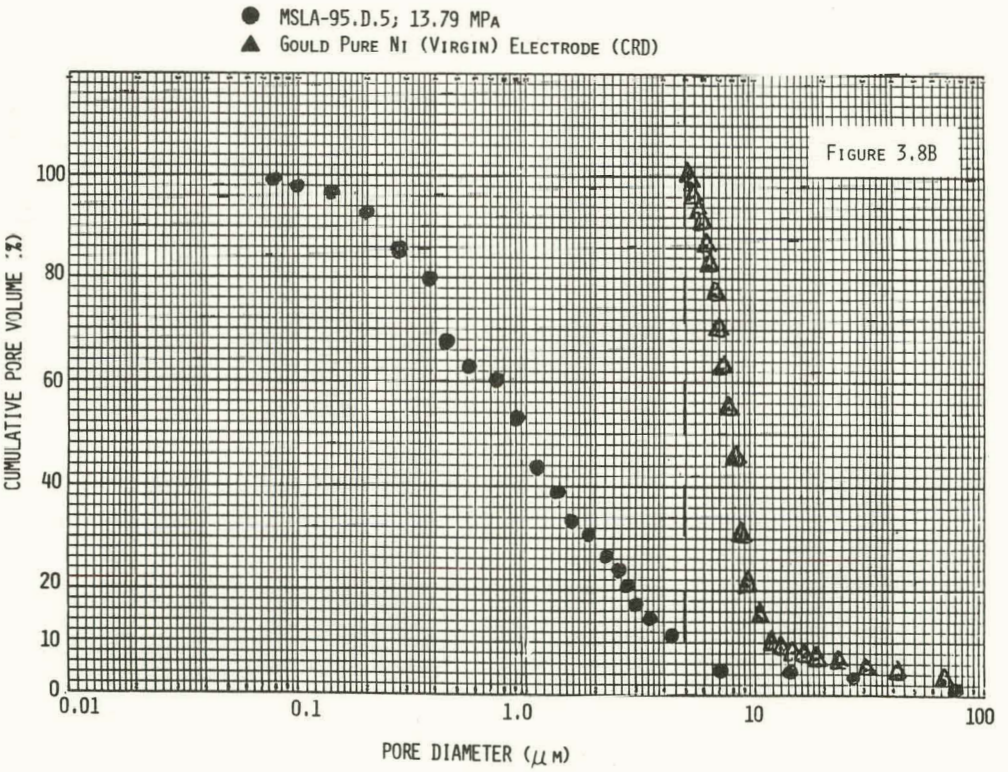

Fig. 3.8 A and B

Porosity Profile Comparisons For $LiAlO_2$ Blank and Electrodes

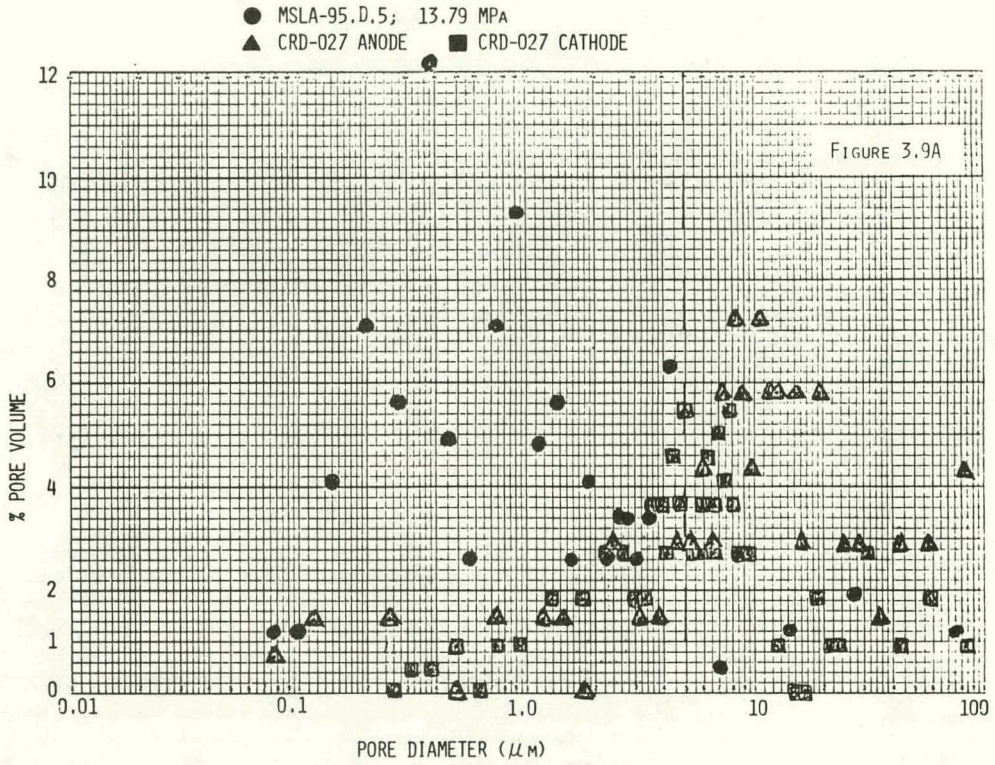

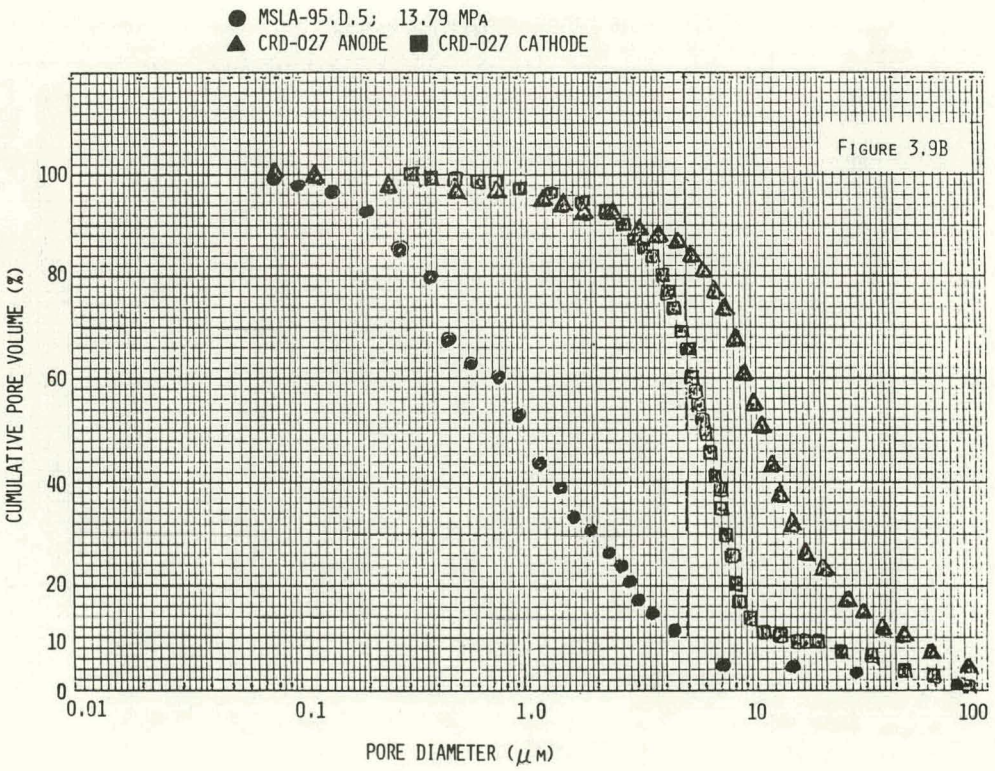

Fig. 3.9 A and B

Porosity Profile Comparisons For $LiAlO_2$ Blank and Electrodes

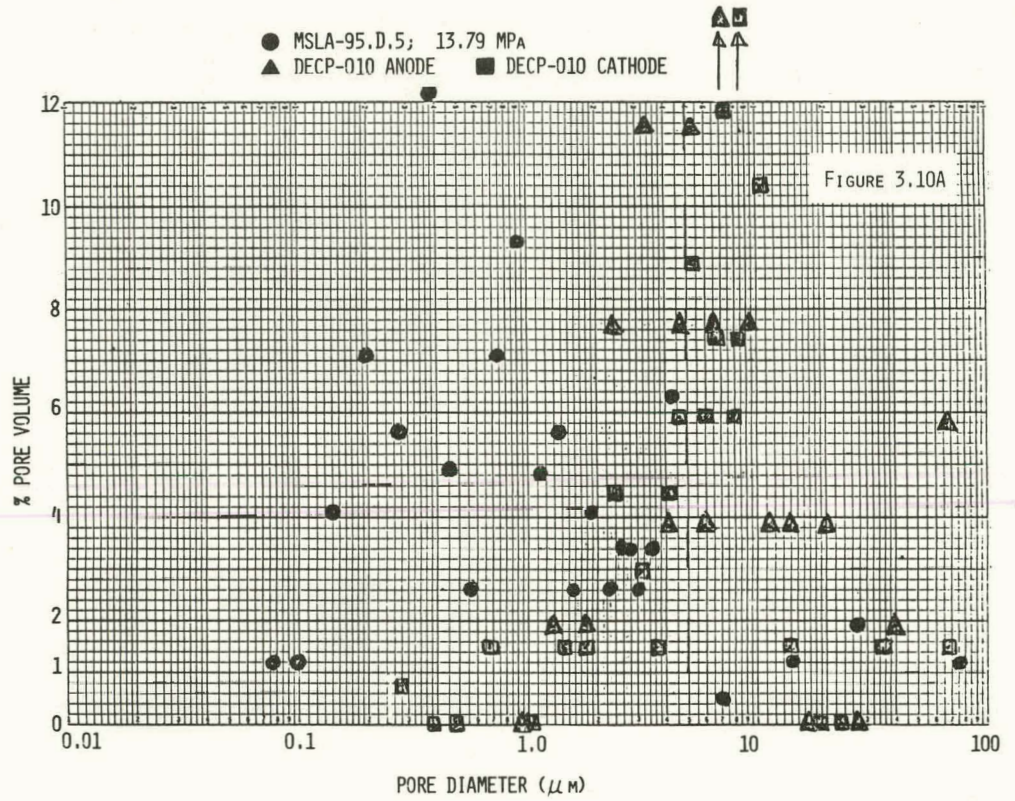

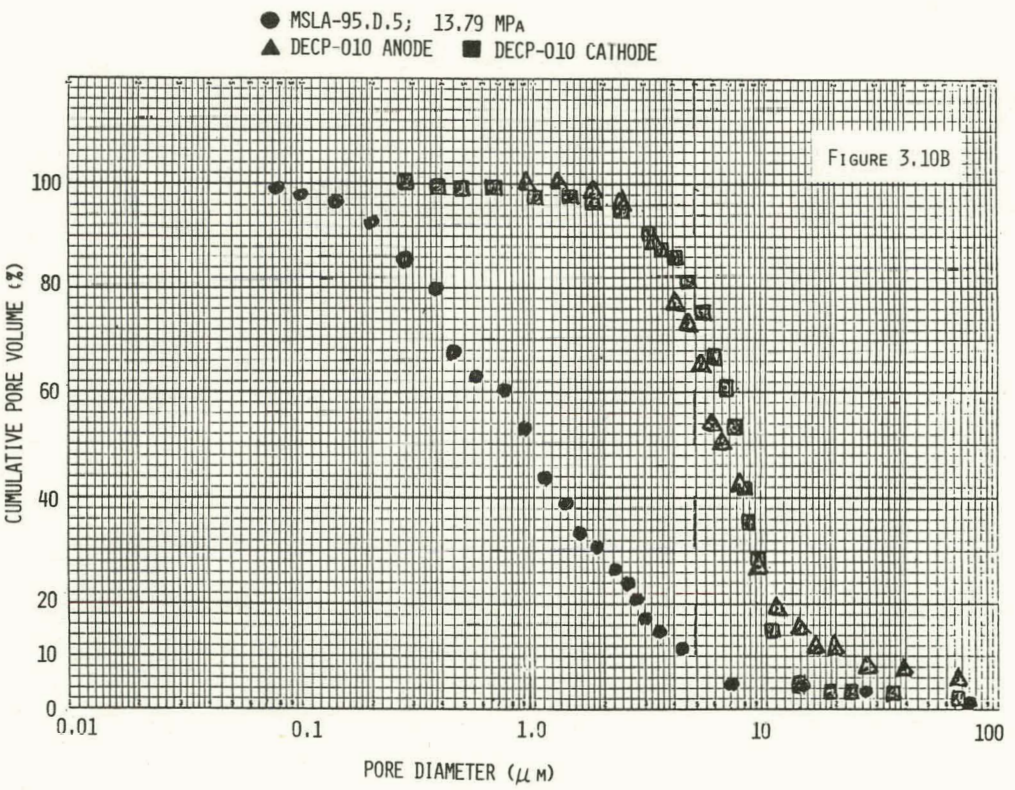

Fig. 3.10 A and B

Porosity Profile Comparisons For $LiAlO_2$ Blank and Electrodes

concluded from these data that electrode flooding, particularly at the cathode, was the source of the poor electrochemical performance of the majority of fuel cell experiments.

It was concluded above that the poor porosity distributions in the $LiAlO_2$ matrices result from highly variable agglomeration of the matrix material, either "chloride" or "conventional" synthesis, during its preparation; the agglomeration is subsequently modified in an unknown fashion by the tile fabrication process. This conclusion was reached, in part, by the examination, in the present context, of a non-$LiAlO_2$ "reference" material. This material was found to be composed of almost totally monodispersed symmetrically shaped crystallites, with a very narrow crystallite size distribution. The average crystallite spherical equivalent diameter for the "reference" material was 0.31μm, compared with values of 0.36 and 0.30μm for the MLSA-95 and MSLA-100 $LiAlO_2$ samples respectively. The $LiAlO_2$ materials did have, however, a somewhat wider range of crystallite sizes which had been anticipated to lead to better packing during pressing and a finer pore size distribution overall.

Figures 3.11A,B show the porosity distribution for a blank of the "reference" material prepared under the same condition as the material in Figure 3.5. The distribution for the "reference" material is distinctly different from that of the $LiAlO_2$ materials. It is well defined, having a distinct peak at ∿0.50μm, with virtually zero porosity above ∿1.0μm. The "reference" material was compared with the used electrodes from experiments CRD-027 (Figures 3.12A,B) and DECP-010 (Figures 3.13A,B). These data indicate that crystallites with an average size near those in the "chloride" synthesis $LiAlO_2$ will, in a monodispersed, narrow size distribution powder, yield porosity distributions which appropriately compliment those of both virgin and used electrode materials. These comparisons again do not consider the effects of crystallite growth in the fuel cell environment. However, the virtually zero overlap indicated in these comparisons gives hope that crystal growth will still allow the appropriate overlap between the distributions.

The de-agglomeration of "chloride" synthesis $LiAlO_2$ was explored so as to allow the realization of matrix porosity distributions akin to those seen with the "reference" material. This effort has taken two approaches. First, modifications to the "chloride" synthesis which reduce, or at least control, the degree of agglomeration were explored. The data on this approach are incomplete at this time.

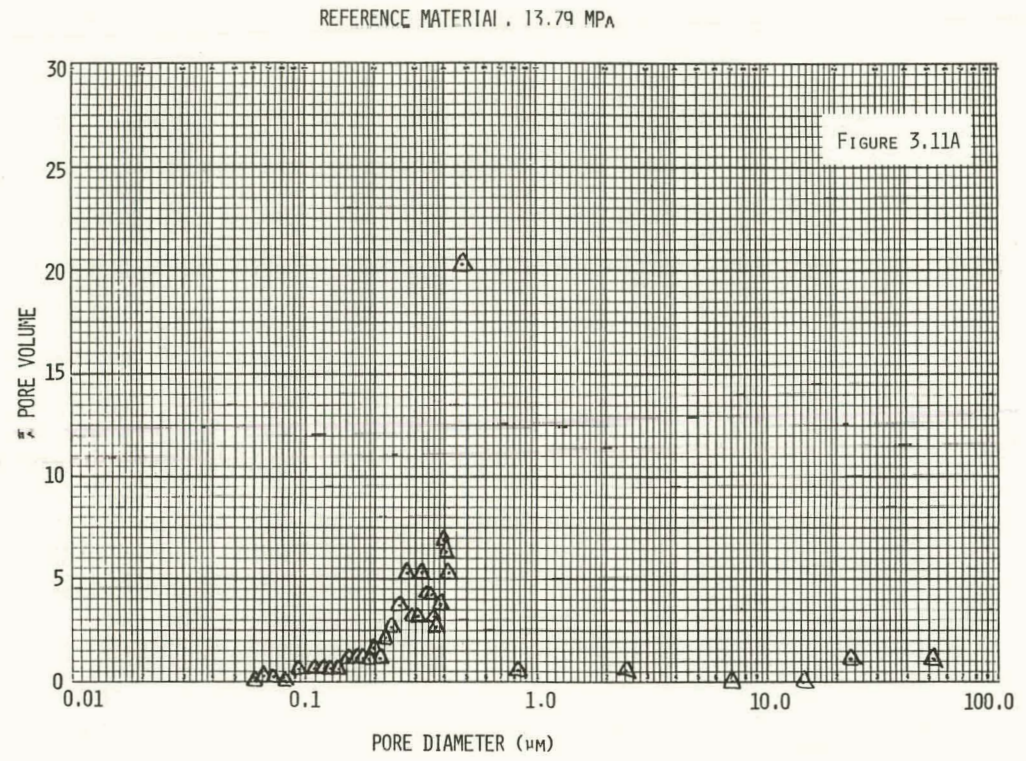

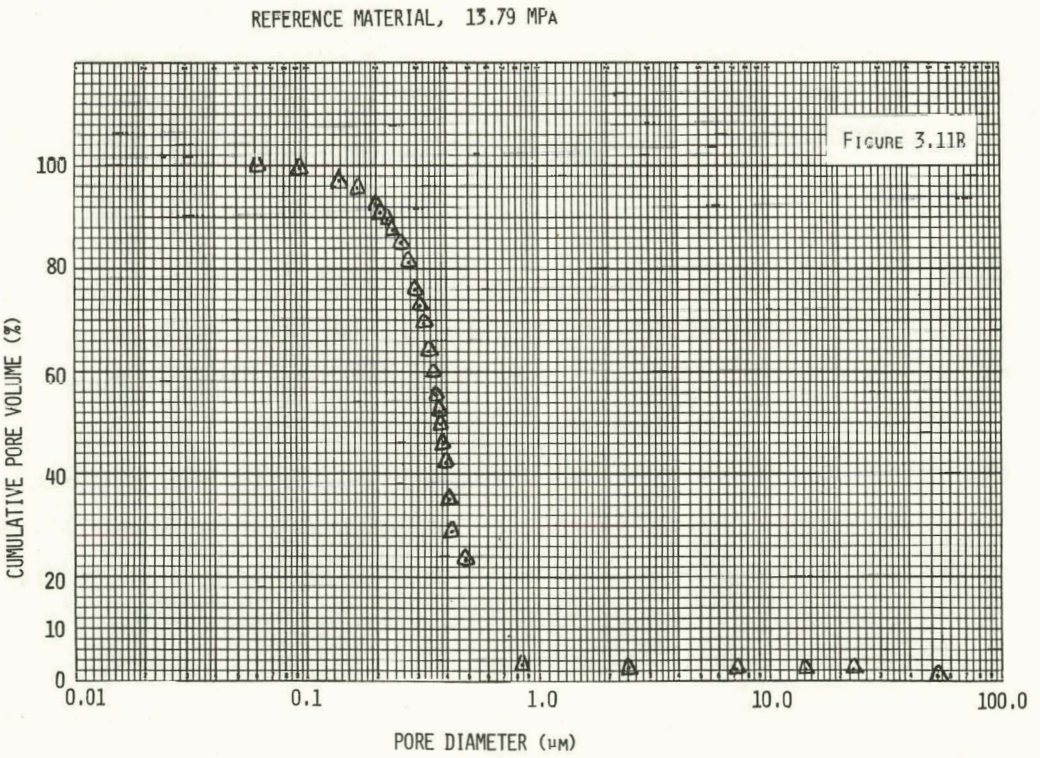

Fig. 3.11 A and B

Porosity Profile For Reference Material

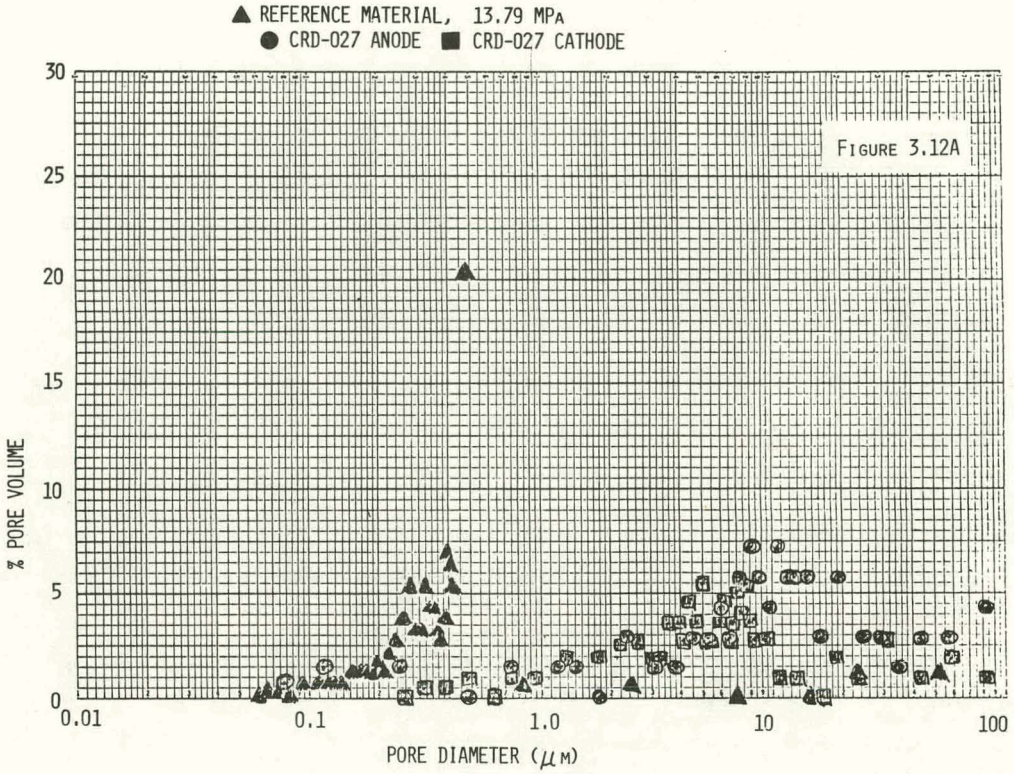

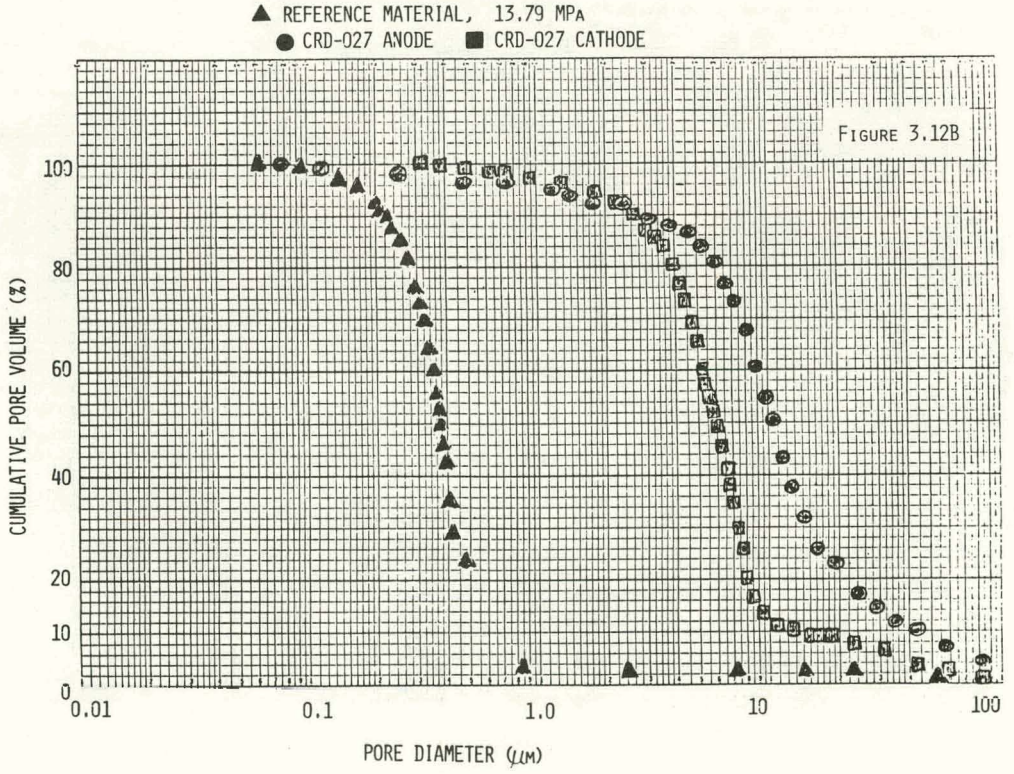

Fig. 3.12 A and B

Porosity Profile Comparisons For Reference Material Blank and Electrodes

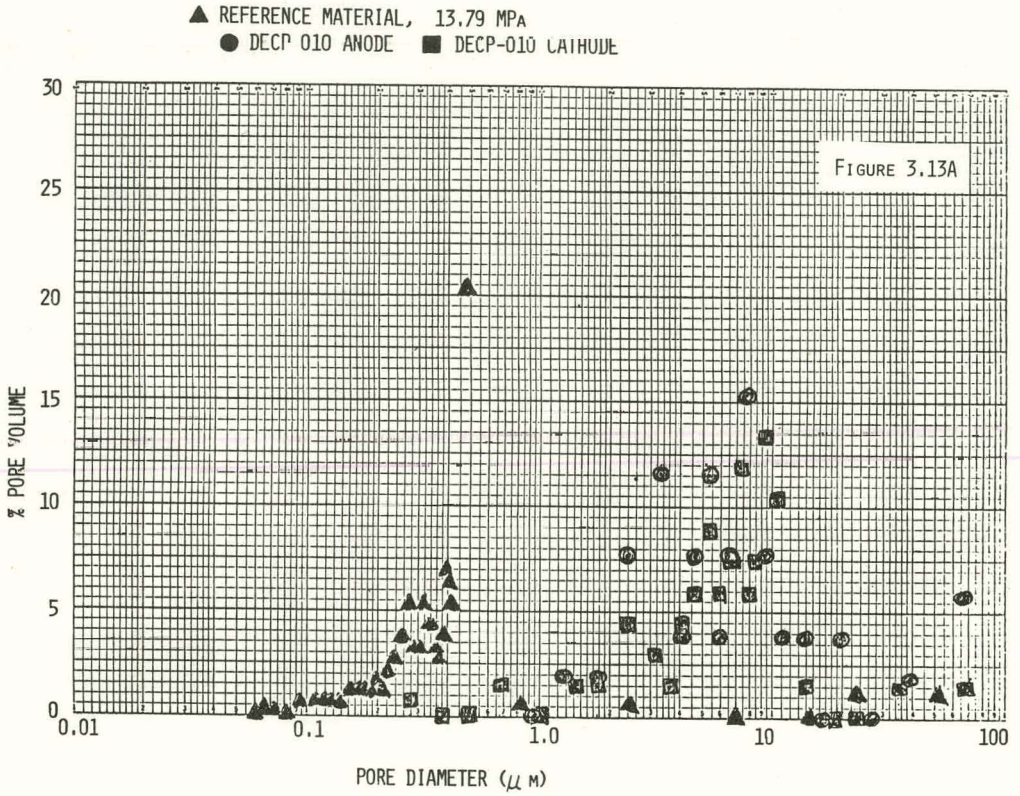

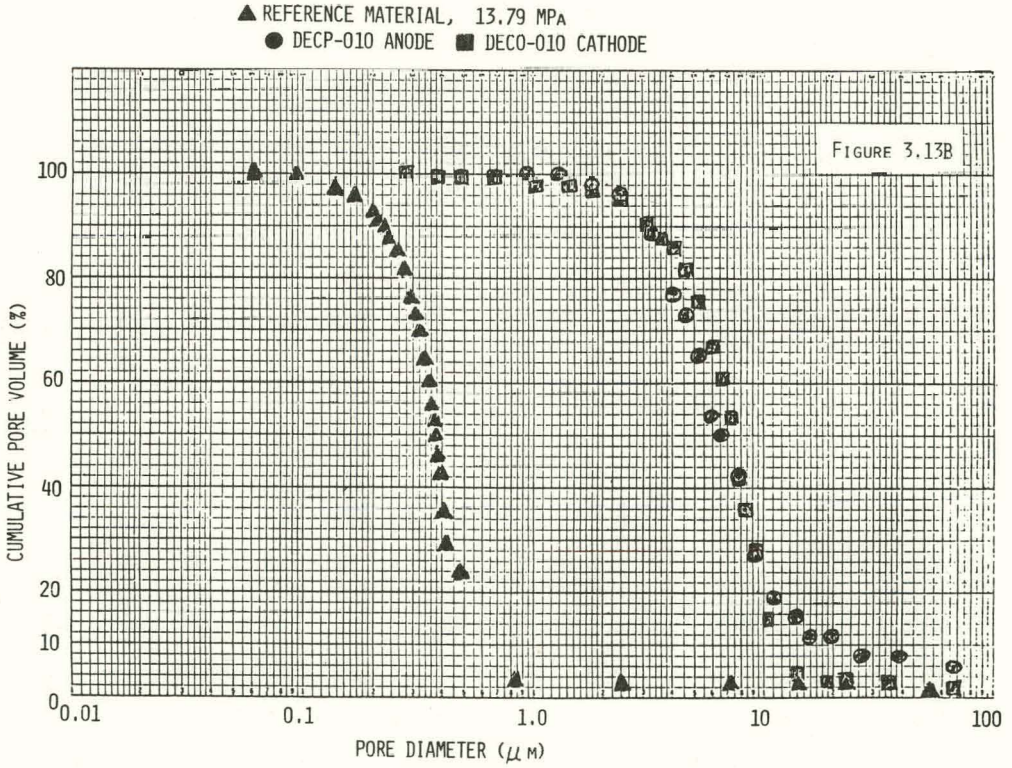

Fig. 3.13 A and B

Porosity Profile Comparisons For Reference Material Blank and Electrodes

The second approach was the modification of agglomerated "chloride" synthesis $LiAlO_2$. Experiments were conducted to determine if a brief vibratory wet milling would de-agglomerate the $LiAlO_2$ without introducing significant contamination or comminuting the individual crystallites. Surface area and porosity measurements indicated that indeed little, if any, crystallite comminution had occurred, but de-agglomeration had not occurred either.

A more rigorous de-agglomeration procedure was then explored. Approximately 1.100 kilograms of "chloride" synthesis $LiAlO_2$ (MSLA-100) was milled for 8 hours in a 4 liter alpha-Al_2O_3 jar mill using technical grade methanol as the vehicle. The resultant slurry was collected and dried by infrared heating in an open dish. A disc sample was pressed at 13.79 MPa, as described above, and its porosity distribution determined. The resultant data are shown in Figures 3.14A,B. These data should be compared with those in Figures 3.7A,B, which is the same lot of $LiAlO_2$ prior to milling. The data of Figures 3.14A,B indicate that milling has sharpened the porosity distribution. There is a well-defined peak at $\sim$0.6 μm and the peak at large diameters ($\geq$10 μm) has been eliminated. Although the distribution is asymmetric, it is broadened toward smaller diameter pores, which is an acceptable situation. The B.E.T. surface area of the milled material was 8.73 meters^2 gram^{-1}, compared with an unmilled value of 7.67 meters^{2}gram^{-1}. These values correspond to a reduction of crystallite spherical equivalent diameter from 0.30 μm to 0.26 μm. This reduction in crystallite size is insignificant compared with the alteration in the porosity distribution. The major consequence of milling has been a reduction in both the number and the size of agglomerates.

A hot-pressing composition, MSLA-100A", has been prepared from the milled $LiAlO_2$. The total porosity measured on the above sample was $\sim$56%, which translates into an electrolyte content of 48 wt% assuming that the compact interstices were just filled with molten electrolyte at the cell operating temperature of 923K. Since electrolyte must be provided for electrolyte wetting and wet seal formation, 800g of hot-pressing composition containing 50wt% predominantly β-$LiAlO_2$-50wt% (62 mole% Li_2CO_3-38 mole% K_2CO_3) was prepared. The $LiAlO_2$, Li_2CO_3 and K_2CO_3 were dry mixed by tumbling overnight in a gallon plastic jug. The electrolyte was impregnated by heating the mixture to 873K for one hour in an air atmosphere using an alpha-Al_2O_3 crucible. The resultant material was a fine powder which passed a 60 mesh nylon screen without comminution. This material will be hot-pressed into electrolyte tiles and evaluated in operating cells.

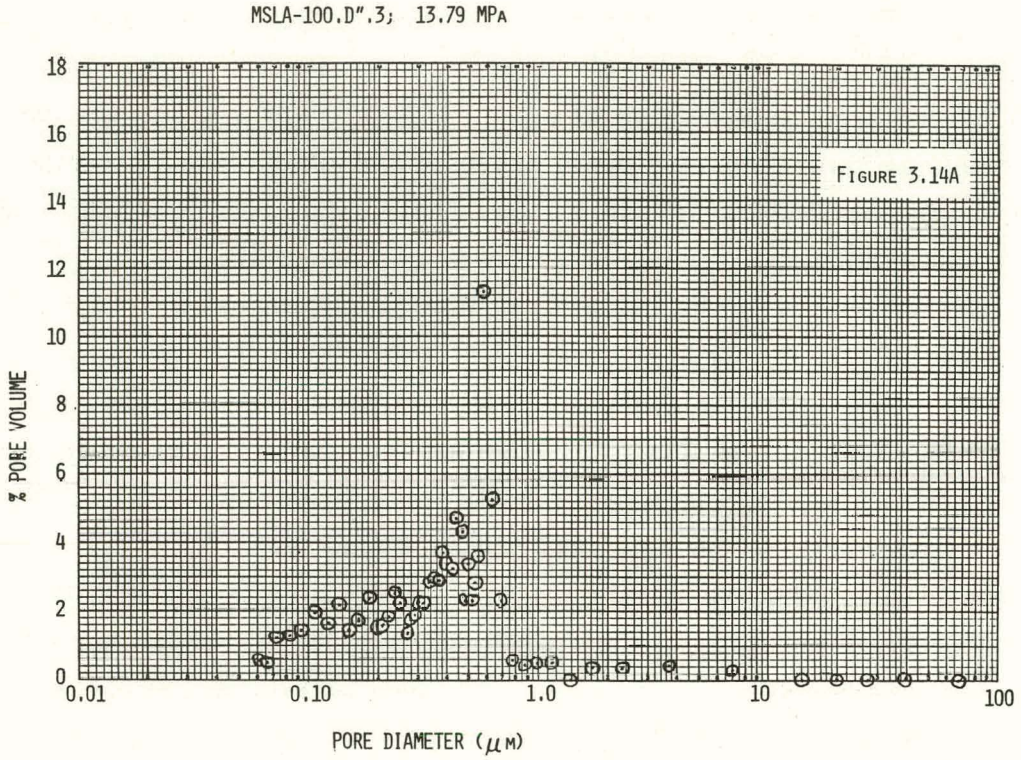

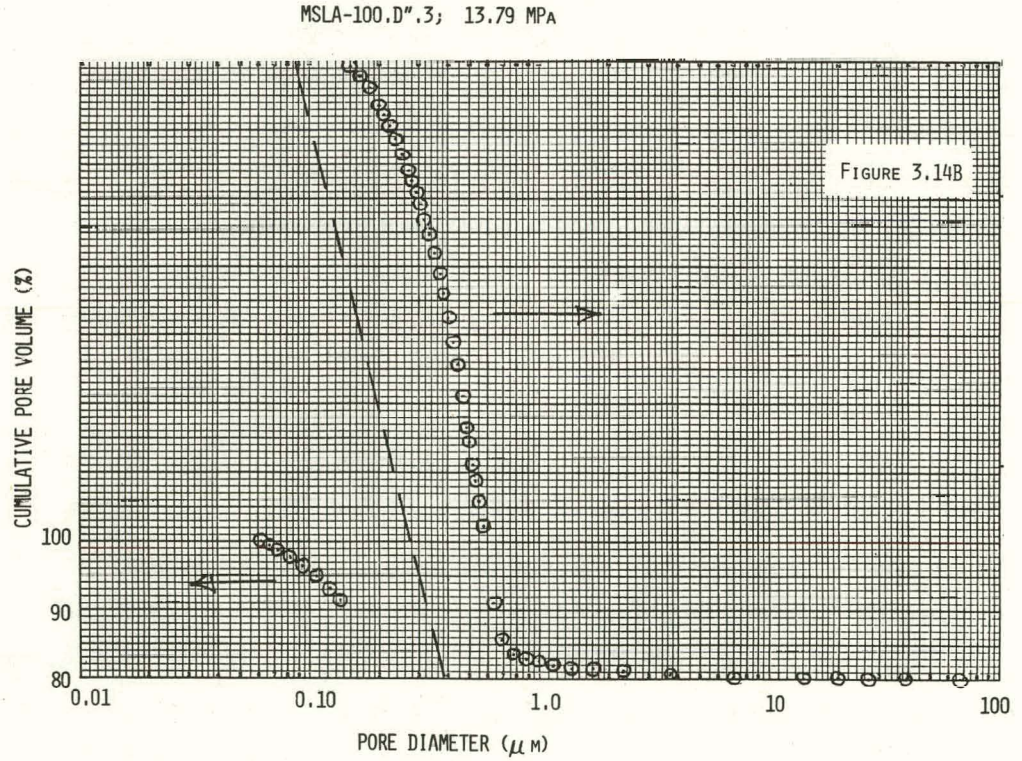

Fig. 3.14 A and B

Porosity Profile of De-Agglomerated $LiAlO_2$

4. ELECTRODE STUDIES

4.1 SUMMARY

During this quarter, a 4000 hour anode sintering experiment was completed. The results quantify the tendency of commercial nickel electrodes to sinter in an anode environment. A second sintering experiment has been initiated, using a closer simulation of the cell environment, and including nickel/chromium electrodes. A new electrode system, employing a 30 mil sintering-resistant nickel/chromium anode and a thinner (15 mil) nickel cathode, has been adapted as the standard for operating cells.

4.2 ANODE SINTERING STUDIES

The 4000 hour anode sintering experiment, described earlier, (4.1) has been completed. The anode materials were: Series G (Gould sintered Ni), and Series S-4, S-5 and S-9, all in-house sintered pure Ni, 80% Ni/20%Cr, and 316 stainless steel, respectively. The methods of sintering the powders into porous plaques and sintering data up to 3,416 hours were reported in the previous quarterly report (4.1). Tables 4.1, 4.2, and 4.3 bring the results to completion of the experiments at 4,017 hours. Figures 4.1 and 4.2 show additional data: in Figure 4.1, data for the electrodes used in experiments CRD-27, CRD-28, and DECP-10 are included. Except for CRD-027, the results were in good agreement with the sintering experiment. In that long-term test the electrodes lost considerably less porosity than the free-standing, isolated coupons of the same material in Series G. Also, Figure 4.2 completes the data for the in-house sintered Ni plaques. This Figure differs from that in the previous report because the final data point for mean free pore size indicates no decrease in pore size, which within the relatively large experimental uncertainty, must be considered constant.

The large extent of shrinkage and loss of surface area of Gould Ni electrode is noteworthy. Although this effect may be attributed to an inherent tendency of porous Ni to shrink, another explanation for the sharp initial decline is the possibility that the Gould electrodes were sintered at low temperature (900°C) in order to obtain high porosity and narrow pore distribution. The Ni powder may also have been derived from chemical reduction and/or decomposition, giving

Table 4.1

Porosity and Pore Size of Sintered Porous Anodes

Sample	Time Hours	Total Porosity	Occluded Porosity	Free Porosity	Mean Free Pore Diameter	Limiting Pore Diameter
		———	Percent	———	Micron	Micron
Gould Sintered Nickel						
G-0	0	74	0	74	6.0	0.9
G-1	168	65	0	65	7.6	1.0
G-2	481	61	1.0	60	7.8	0.6
G-3	835	51	14.2	37	7.0	0.1
G-4	1,357	43	14.4	29	9.1	0.2
G-5	2,915	28	0	28	14.3	0.2
G-6	3,416	38	11.7	26	10.7	1.6
G-7	4,017	22	0	22	9.9	2.0
CRD Sintered Nickel (Source: Inco No. 255)						
S4-0	0	65	4.5	60	8.3	0.8
S4-0	0	67	1.9	65	10.2	1.6
S4-1	168	59	3.3	56	10.5	2.9
S4-4	1,357	55	10.2	45	10.2	0.2
S4-5	2,915	66	4.7	61	23.0	0.2
S4-6	3,416	48	5.8	43	7.8	0.1
S4-7	4,017	50	6.6	43	12.6	2.9
Sintered Nichrome Alloy (Source: AEE-Ni 225)						
S5-0	0	52	3.3	49	9.6	3.4
S5-1	168	50	1.5	49	8.0	0.6
S5-2	481	49	3.6	43	7.4	1.6
S5-4	1,357	49	5.2	44	7.2	0.7
S5-5	2,915	50	5.1	45	6.7	0.1
S5-7	4,017	53	8.4	45	7.1	0.3
CRD Sintered Stainless Steel (Source: AEE-SS 147)						
S9-0	0	55	0	54	11.6	1.5
S9-1	168	56	12	44	9.5	0.6
S9-2	481	54	14	40	7.7	0.1
S9-4	1,357	56	18	38	6.5	0.2
S9-5	2,915	56	24	32	8.1	0.7
S9-6	3,416	54	28	26	6.8	0.3
S9-7	4,017	58	19	39	7.4	0.4

Table 4.2

Surface Area And Its Changes During Sintering of Anodes

Sample	Time Hours	Surface Area (cm^2/g)	Change At Const. Porosity %	Actual Porosity Change %
Gould Sintered Nickel				
G-0	0	1120	0	0
G-1	168	887	-21	-32
G-2	481	864	-23	-37
G-3	835	--	--	--
G-4	1,357	740	-33	-74
G-5	2,915	471	-58	-84
G-6	3,416	630	-44	-80
G-7	4,017	681	-39	-82
CRD Sintered Ni				
S4-0	0	736	0	0
S4-1	168	642	-13	-21
S4-4	1,357	661	-10	-36
S4-5	2,915	293	-60	-61
S4-6	3,416	864	+17	-20
S4-7	4,017	535	-27	-50
CRD Sintered Nichrome Alloy				
S5-0	0	730	0	0
S5-1	168	876	20	0
S5-2	481	947	30	28
S5-4	1,357	979	34	31
S5-5	2,915	1046	43	40
S5-7	4,017	987	35	23

Table 4.3

Shrinkage of Porous Anodes

Sample	Time Hours	Anode Dimensions Length	Width	Thickness	Shrinkage From Geometry	Density
		cm			percent	
Gould Sintered Ni						
G-0	0	2.72	0.520	0.127	0	0
G-1	168	--	--	--	--	-12
G-2	481	--	--	--	--	-21
G-3	835	2.70	0.480	0.117	-16	-19
G-4	1,357	2.54	0.476	0.114	-23	23
G-5	2,915	2.54	0.317	0.117	-48	-29
G-6	3,416	2.60	0.470	0.107	-27	-25
G-7	4,017	2.55	0.470	0.102	-32	-31
CRD Sintered Ni						
S4-0	0	2.70	0.60	0.082	0	0
S4-1	168	--	--	--	--	--
S4-4	1,357	2.60	0.62	0.069	-16	-7
S4-5	2,915	2.50	0.50	0.063	-41	0
S4-6	3,416	2.60	0.59	0.082	-5	-11
S4-7	4,017	2.62	0.60	0.066	-25	-11
CRD Sintered Nichrome Alloy						
S5-0	0	2.70	0.73	0.132	0	0
S5-1	168	2.70	0.70	0.132	+4	+1
S5-2	481	2.70	0.76	0.130	-3	+3
S5-4	1,357	2.73	0.71	0.127	+5	+2
S5-5	2,915	2.71	0.77	0.136	-9	+2
S5-7	4,017	2.72	0.74	0.135	-4	0

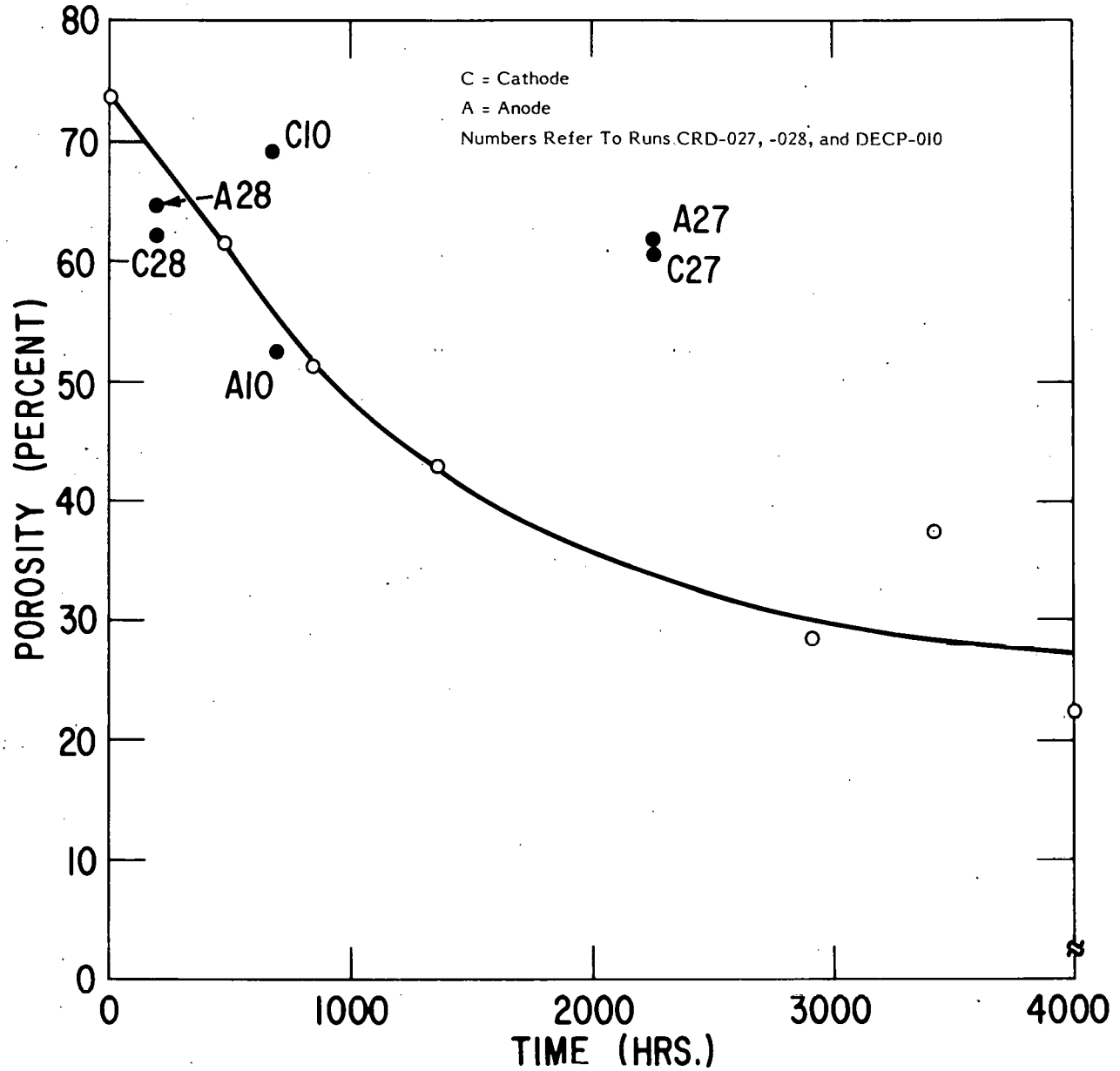

Fig. 4.1

Comparison of In-Cell and Out-of-Cell Electrode Porosity Change with Time

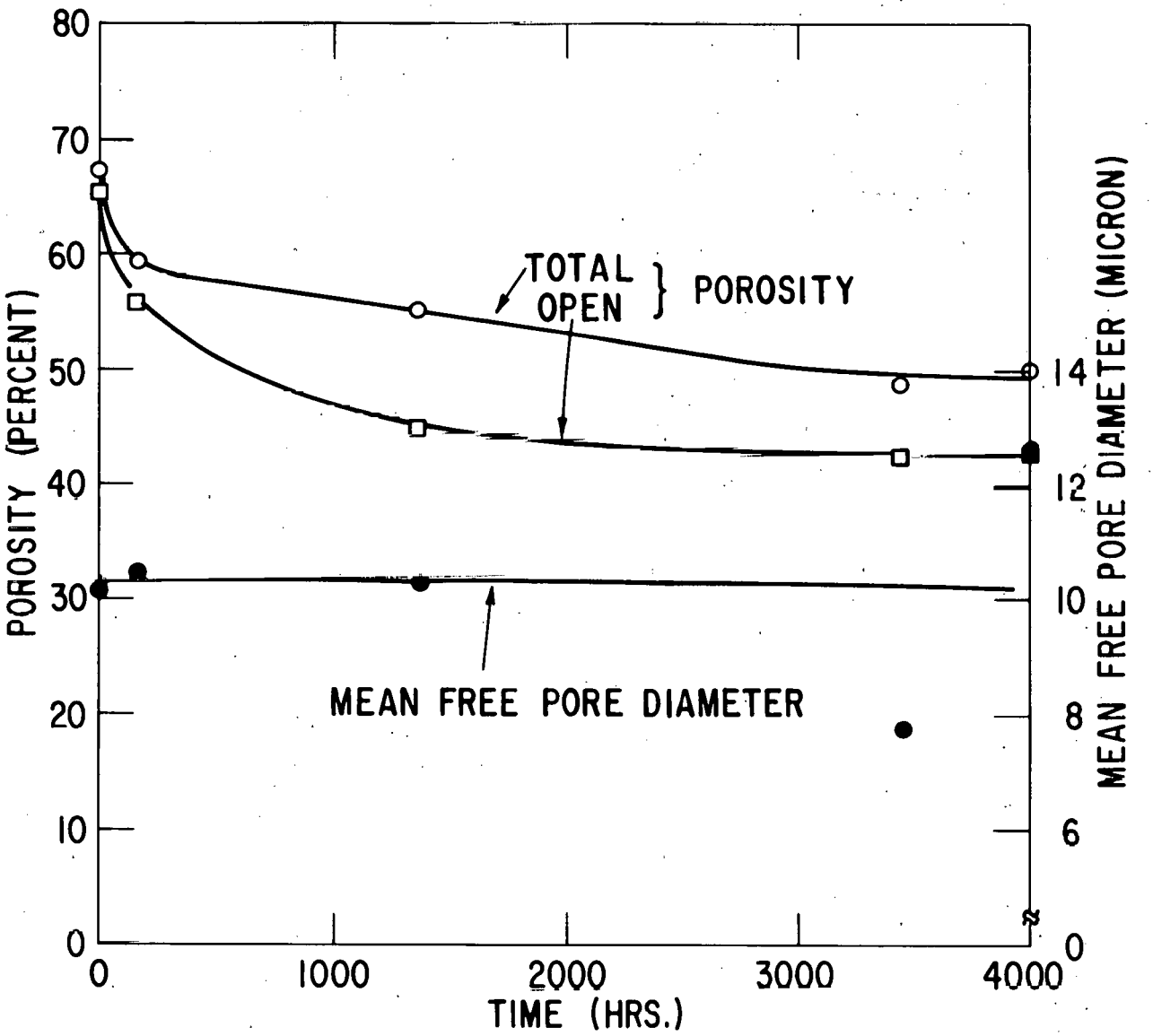

Fig. 4.2

Change in Nickel Electrode Porosity with Time

irregular particle surfaces which may have been carried over to some extent to the sintering experiment with the same shrinkage effect. For these reasons sintering experiments for Ni and Ni/Cr alloys are being repeated in a second experiment with a known source of Ni and with mechanical restraint on the porous plaque.

In the second sintering experiment, a vertical sintering furnace, for use at 650°C, was assembled with provisions for storing samples in an open stainless steel wire tray. The new sequence of tests was started 2/6/79 and comprises the following four types of samples.

Series 21: Gould Porous Pure Ni/0.056 cm thick

Series 22: Gould 90% Ni/10Cr/0.078 cm thick

Series 13: GE Porous Pure Carbonyl Ni (INCO No. 255)/0.071 cm thick

Series 14: GE 90%Ni/10Cr/0.074 cm thick

In the first experiment, the samples were exposed to the fuel gas mixture (24% CO_2, 34% H_2, 42% N_2) at 650°C in an isolated condition. In the second experiment, at the same temperature and in the same gas, the porous electrode samples are sandwiched in the array: stainless steel screen/porous Ni or NiCr electrode/electrolyte tile/stainless steel screen. This corresponds more closely to the actual electrode operation.

In preparation for the sintering experiment, a few porous Ni/Cr plaques were sintered by prefiring the Ni-Cr mixture, consisting of 90 weight % INCO No. 255 carbonyl Ni and 10% reagent grade chromium powder, at 500°C for 30 min., followed by sintering at 1050°C for 30 min. An example is the 90/10 Ni/Cr electrode with 46% porosity and 4.6 microns mean pore size whose pore distribution is shown in Fig. 4.3.

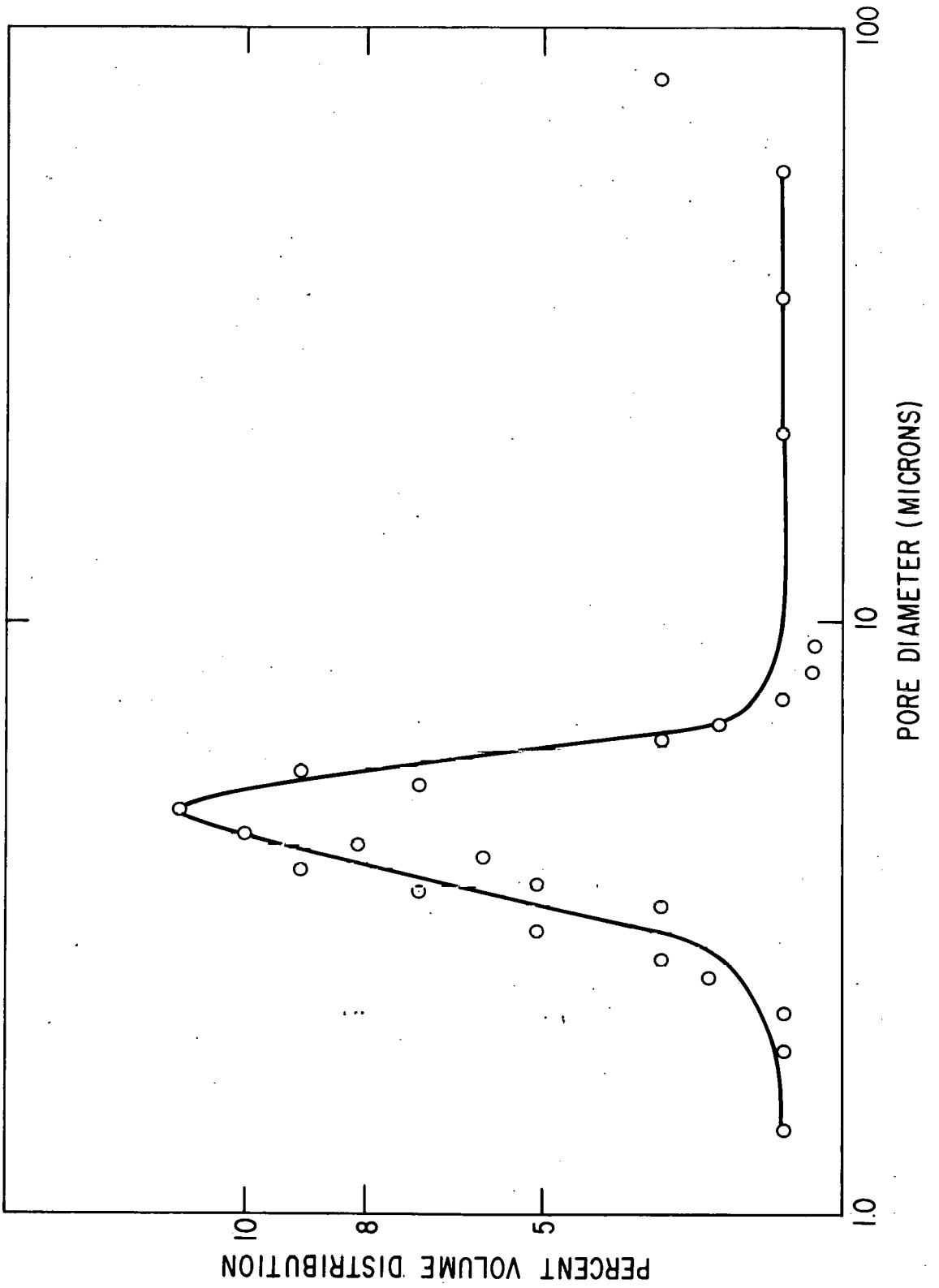

Fig. 4.3

Porosity Profile for Nickel/Chromium Anode

4.3 NEW ELECTRODE SYSTEM

As discussed in Section 2, a new electrode system is now being employed as the "standard" electrode system for cell performance testing. The electrodes, obtained from Gould, are as follows:

Anode: 0.030" Thick, Nickel Plus 10% Chromium, 65% Porosity, 4.6μ Average Pore Size

Cathode: 0.015" Thick, Nickel, 80% Porosity, 8.5μ Average Pore Size

5. CONTAMINANT TOLERANCE

5.1 SUMMARY

The principle goals of this activity are to determine the effects of various contaminants on state of the art cells and to establish tolerance levels of molten carbonate fuel cell components for these contaminants. The primary efforts during this quarter have been focused on the effects of H_2S in the fuel gas and HCl in the anode and cathode gas on the performance of cells under constant load conditions.

Studies of the effects of H_2S under non-sulfidizing conditions at the nickel anode continue to be hampered by the lack of suitable cell design. Alternative cell designs are being pursued and two different approaches appear promising.

Two experiments have been pivotal in the study of the effects of HCl. In one experiment, a cell which ran on our standard fuel with 10 ppm HCl added showed marked deterioration in performance after 24 days of running. A second experiment, which ran with 100 ppm HCl added to both the fuel and oxidant, showed a drastic drop in performance shortly after being placed on HCl; in addition, severe corrosion of the cathode compartment, resulting in almost complete plugging of the gas passages in the current collector plate, was observed.

5.2 EFFECTS OF H_2S ON CELL PERFORMANCE AND COMPONENTS

Although the effects of sulfidation of nickel at high sulfur activities in the anode gas have been substantiated, attempts to extend the experiments to include the effects of low sulfur activities in the fuel gas have been hampered either by sulfidation of the stainless steel hardware or by poorly performing anodes. In order to alleviate these problems, two approaches have been taken during this reporting period.

The first approach has been to eliminate the effect of stainless steel while still employing the 3" x 3" cell design by nickel-plating the stainless steel hardware and using a nickel current collector plate. Also, as mentioned in previous reports, sulfidation of the inlet and exit tubes is a problem because of the

increased stability of sulfides at lower temperatures. For example, Figure 5.1 shows the theoretical concentration of H_2S required for sulfidation of nickel and iron in the presence of our standard fuel as a function of temperature. The changes in slope of the nickel curve are due to the formation of a non-stoichiometric $Ni_3S_{2\pm x}$ above $\sim$ 535°C and to the formation of a liquid nickel-sulfide/nickel eutectic above ~620°C. It can be seen that with our 100 ppm gas below ~600°C the stainless steel will sulfidize and below ~550°C the nickel will sulfidize. In order to prevent the sulfidation of the inlet tubes, the anode gas streams were fed through Al_2O_3 sleeves inside the nickel plated stainless steel tubes.

Cell CRD042 employed this nickel-plated, Al_2O_3-sleeved hardware. The cell used 0.050" nickel anode and cathode, and a 0.100" tile pressed from Q-13 powder. The cell was operated with our standard fuel at 100 cc/min under a current load of 50 ma/cm^2 corresponding to a fuel utilization of 50%. On day 3, 100 ppm H_2S was added to the fuel while all other operating conditions remained constant. These conditions do not represent a nickel sulfidation region and, indeed, no change in either cell performance or open circuit potential was observed. Analysis of the exit gas stream for H_2S, however, revealed only 2 ppm H_2S in the exit stream. The cell was returned to open circuit and maintained with a constant flow of 100 ppm H_2S-containing fuel for eleven days at open circuit. The exit gas stream H_2S concentration never exceeded 45 ppm H_2S during this eleven day period. The open circuit voltage began to drop after day 10 and by day 11 a sizeable cross leak had developed; the cell was shut down. Post-mortem analysis of this cell showed evidence of corrosion and sulfidation in two areas of the anode. The gas side of the anode was still light gray with the exception of the area of the cross leak where a black material (NiO probably) had formed in a pattern corresponding to a crack. The electrolyte side of the anode was completely darkened. Analysis is presently being carried out to determine the composition of this black material. An additional observation from CRD042 was severe sulfidation at the cell end of the anode inlet tube; it is likely that the thin Al_2O_3 feed tube did not allow the gas temperature at the nickel/Al_2O_3 tube interface to reach 650°C. Sulfidation, enhanced at lower temperatures, thus occurred at this interface due to the lack of adequate preheat of the gas. This cell design is presently being altered to include a preheat system which is stable to sulfur.

The second approach to facilitating the study of sulfur effects has been the design of a suitable 2.5 cm^2 Al_2O_3 cell. The initial cell design is shown in

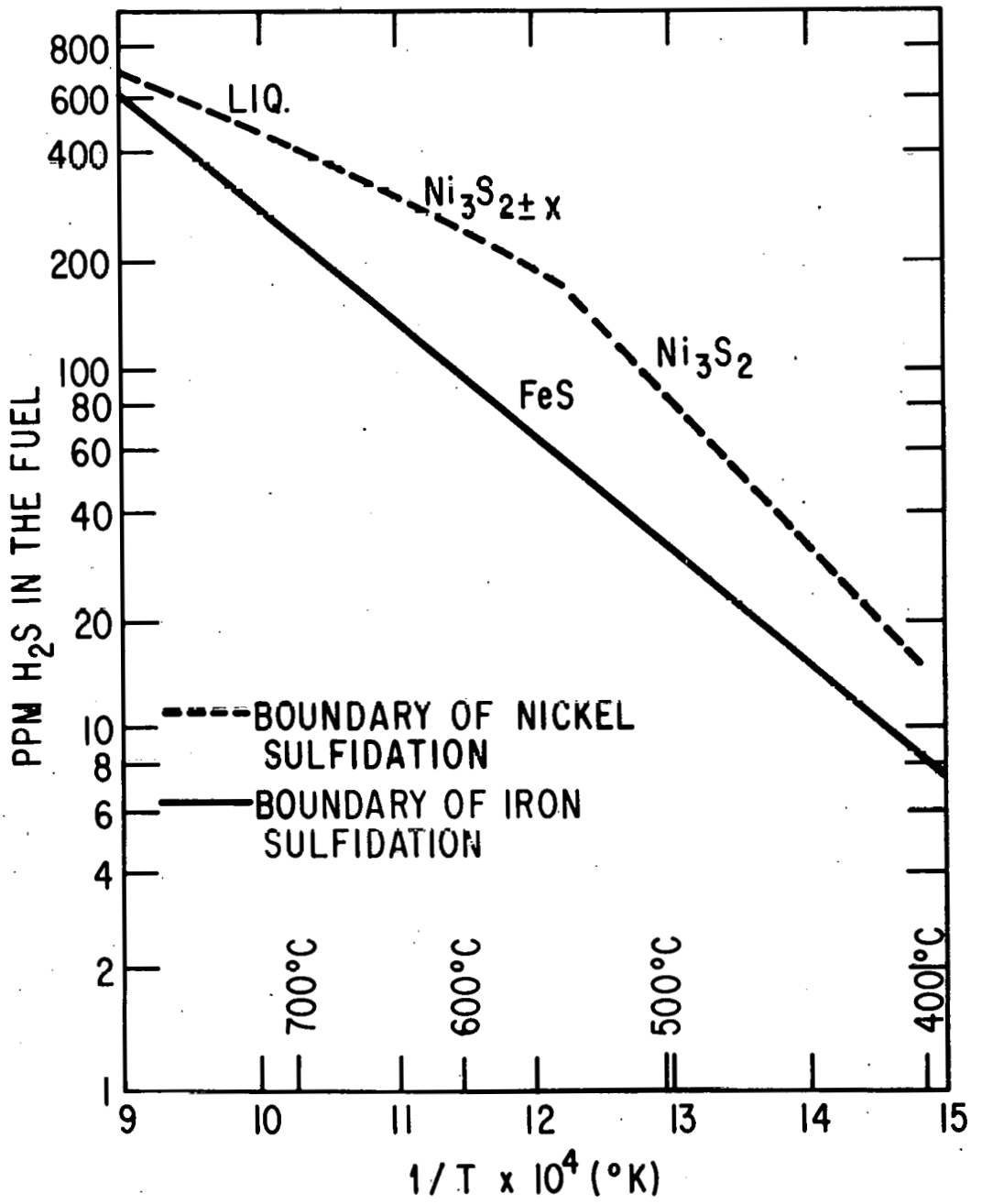

Fig. 5.1

Temperature Effect on Sulfidation of Nickel and Stainless Steel

Figure 5.2. In this design the entire cell, with the exception of electrodes and current collector ring, is Al_2O_3. The current collector ring is a .002" Au foil. Electrical connection to the Au foil is made with Au wire which exits the cell via the inlet and exit gas tubes. In order to improve the gas analysis and eliminate long lag times of any compositional changes in the gas, this cell has only a 3 cm^3 gas chamber.

Two runs, CRD AL-1 and CRD AL-2, have been made in this cell. Both runs failed due to lack of an adequate wet seal. It has become apparent that the new aqueous slurry process tiles which we are employing are very rigid and require very close tolerances. Closer examination of the cell design showed misalignment and uneveness in the Al_2O_3 collars which made the sealing difficult. Also, there is very little wet seal area in the region of the reference tubes. This cell is being resurfaced at present to improve its sealing capabilities.

A second Al_2O_3 cell design, shown in Figure 5.3, has been constructed to eliminate the difficulties with the first design. The primary difference between the two designs is that the top half of the new cell fits inside its bottom half while still forming a wet seal with the tile. This feature eliminates alignment problems encountered with the first design. The second difference is that this new design has only a .012" interruption in the wet seal due to the reference electrodes. This design is presently under test.

5.3 EFFECT OF HCl ON CELL PERFORMANCE AND COMPONENTS

5.3.1 Experimental

All cell tests used our standard 3" x 3" stainless steel cells. Anodes and cathodes were 44 cm^2 active area Gould sintered nickel electrodes. Cell CRD036, preliminary results of which were reported last quarter, used 50 mil thick anode and cathode. Cell CRD049 employed a 30 mil thick anode and a 15 mil thick cathode. The tile was ~75 mils thick, pressed from P-27M aqueous slurry process powder. The pure fuel gas was our standard 34% H_2, 24% CO_2, 42% N_2 which at 650°C yields .2228 H_2, .1228 CO_2, .1177 H_2O, .1177 CO, bal. N_2. In order to introduce 100 ppm HCl into our standard fuel, the gas was bubbled through a 16 wt % HCl solution maintained at 26°C. The new equilibrium gas composition at 650°C is thus .2146 H_2, .1258 CO_2, .1072 CO, .1359 H_2O, 100 ppm HCl, bal. N_2. The pure oxidant gas was 70% H_2O, 30% CO_2. This gas was also bubbled through a 16 wt % HCl solution at 27°C to provide a flow of 100 ppm HCl to the cathode. The gas flow rates at the anode and cathode were 100 cc/min and 300 cc/min.

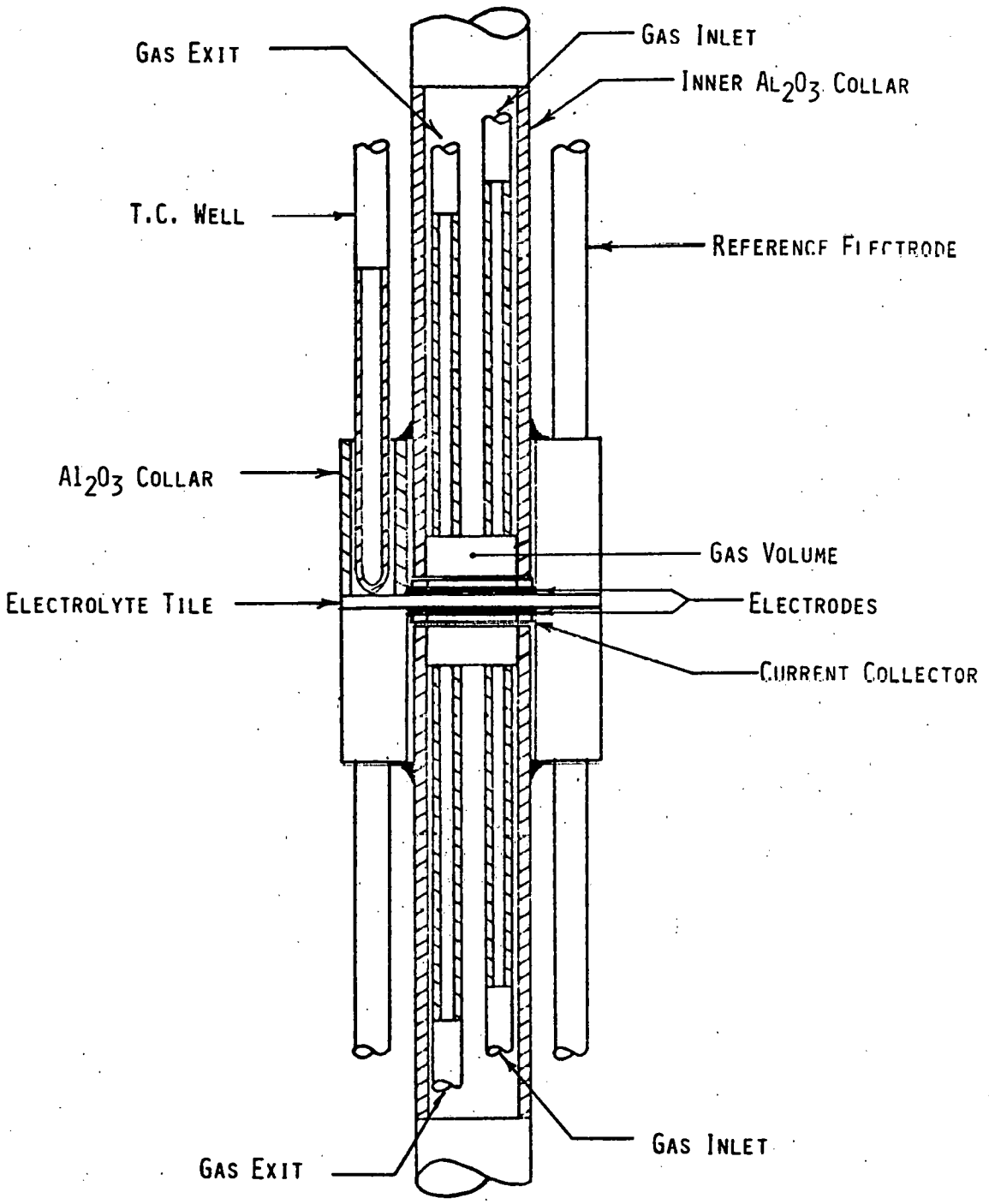

Figure 5.2 -- Initial 2.5 cm^2 Active Area Alumina Cell Design

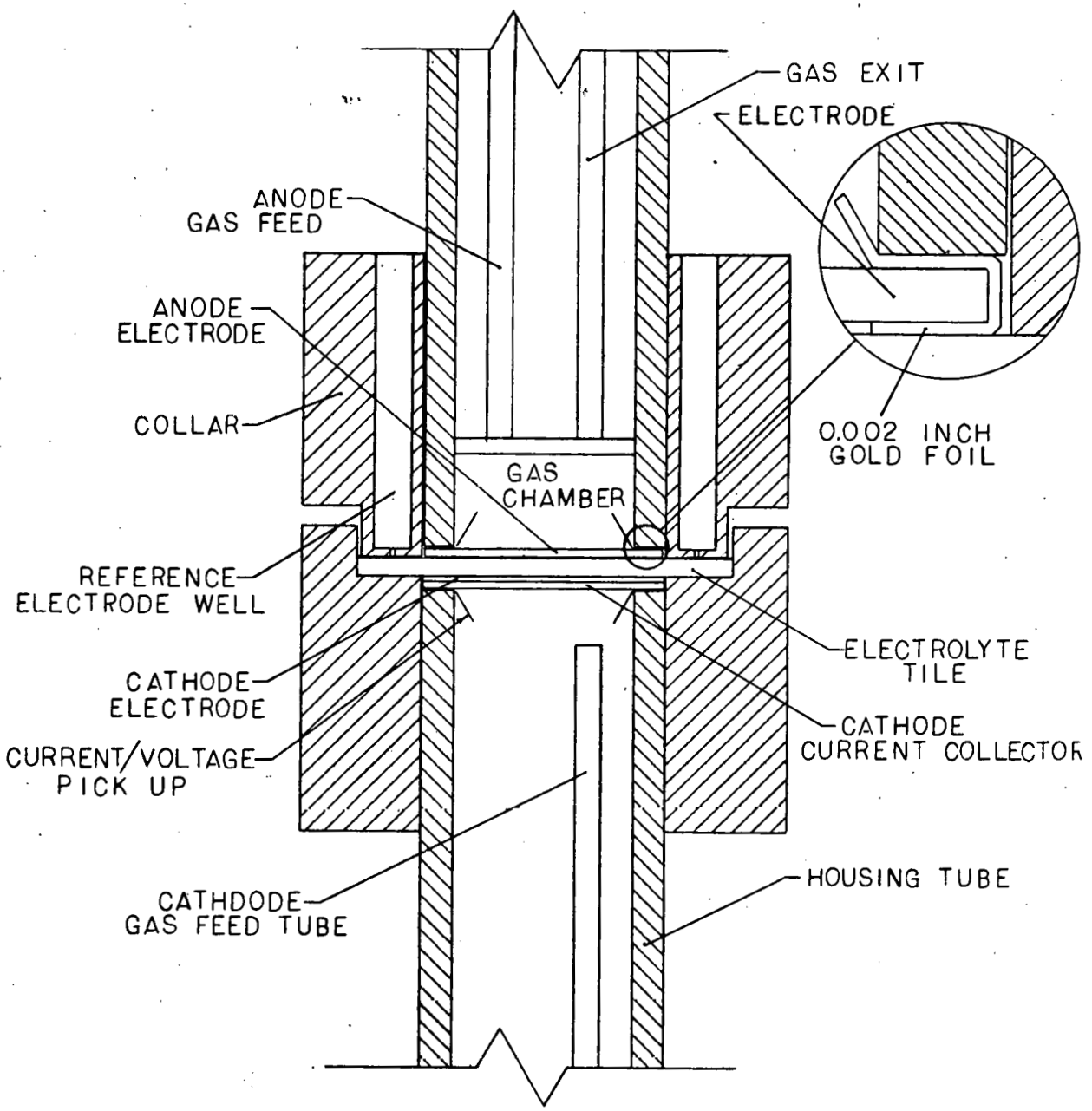

Figure 5.3 -- Revised 2.5 cm^2 Active Area Alumina Cell Design

5.3.2 Results

As reported earlier, cell CRD036 was run for 28 days with 10 ppm HCl added to the fuel gas. The stained sections of the tile from that run were analyzed by E.D.A. and x-ray diffraction. Results revealed the presence of HCl and LiCl and/or $LiAlOCl_2$. The latter two phases have similar structure and lattice. Although there was a serious performance decay (see Figure 5.4) after 26 days, the decay could not be linked directly to the effect of the HCl on the tile. The decay may have been due to continued cell operation at the low cell potential.

A new cell, CRD049, was put on test with 100 ppm HCl added to both anode and cathode gas. This cell ran for 8 days on pure gases at 50 ma/cm^2, corresponding to 50% utilization of the fuel and 15% utilization of the oxidant. On day 8 both gas streams were bubbled through 16 wt % HCl solution to pick up 100 ppm HCl. The cell was then run at constant current (50 ma/cm^2) for 6 days. During this period, the cell was returned to open circuit for 1/2 hr. periods while a daily polariztion curve was taken. At day 14 the cell was put on a constant potential load of .700 volts since the cell potential at 50 ma/cm^2 had dropped below .700 volts. Shown in Figure 5.5 are cell voltage data as a function of time for this cell. The voltage data reported are: $E_{C/A}$ (O.C.), the open circuit cell potential after 1/2 hour at open circuit; $E_{C/A}$ (P), the cell potential at 50 ma/cm^2 taken from the polarization curve after 1/2 hour on open circuit; $E_{C/A}$ (L), the cell potential at 50 ma/cm^2 after 24 hours of constant load; $E_{A/R}$ (P), the anode/reference voltage at 50 ma/cm^2 taken from the polarization curve; and $E_{A/R}$ (L), the anode/reference voltage at 50 ma/cm^2 after 24 hours of constant load. The reference for this cell was .1486 O_2/.30 CO_2//Au which is at the same theoretical potential as the cathode. As can be seen from Figure 5.5 there is a drop in performance for this cell at day 8 corresponding to the introduction of HCl; the drop increases in severity through day 14 when the cell was put on constant potential load. The drop in open circuit potential, also observed at day 8 can be explained due to the dilution of the gases by water and HCl from the saturator: the theoretical cell potential is

$$E_{C/A} = 1.022 - \frac{RT}{nF} \quad \ln \frac{(a_{H_2O})(a_{CO_2})}{(a_{H_2})(a_{CO_3^{=}})} \text{ anode} + \ln \frac{(a_{CO_3^{=}})}{(a_{O_2})^{1/2}(a_{CO_2})} \text{cathode}$$

which for our pure gases becomes:

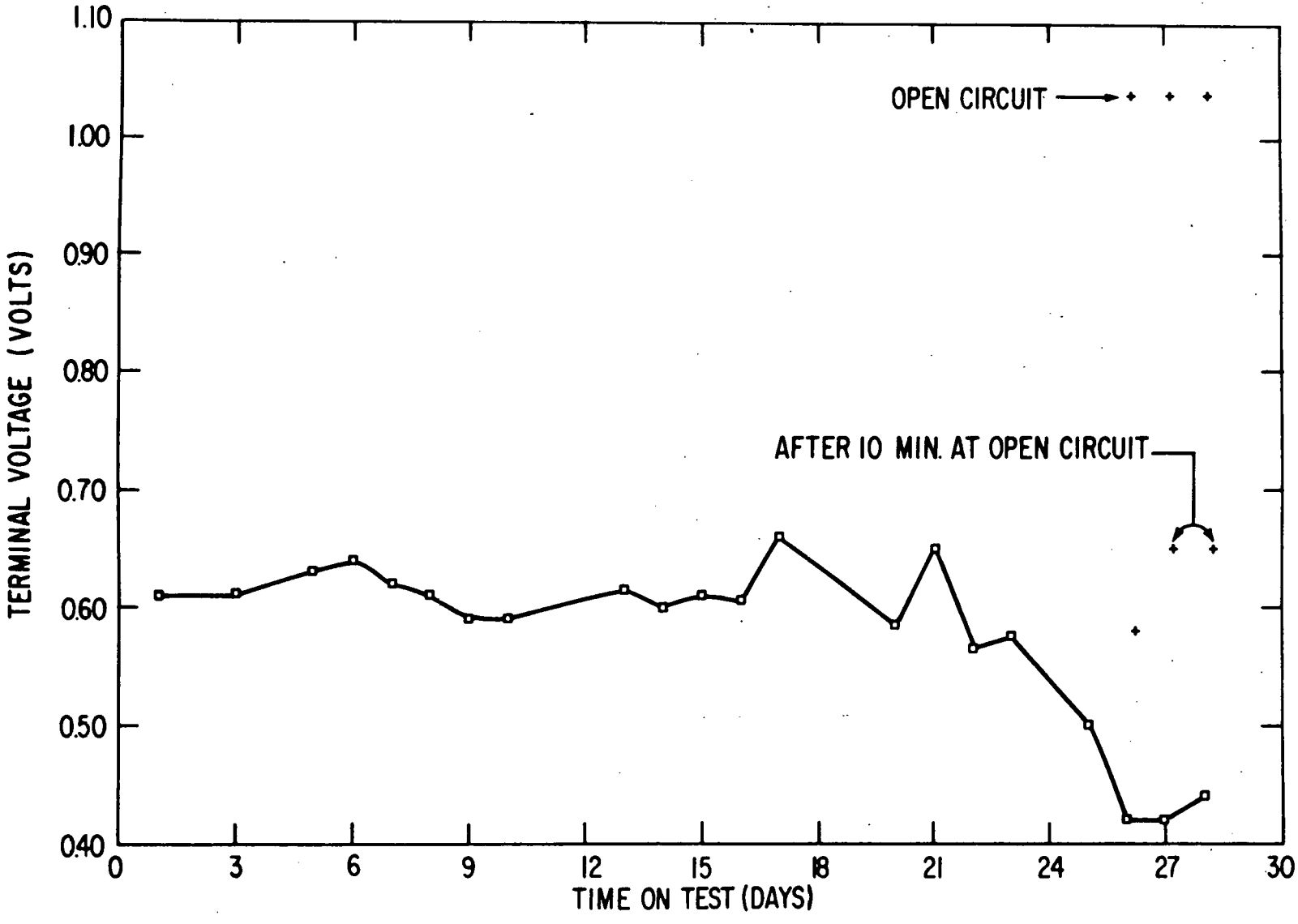

Figure 5.4 -- CRD036 Cell Voltage At 3.1 Amps As A Function Of Time On Load

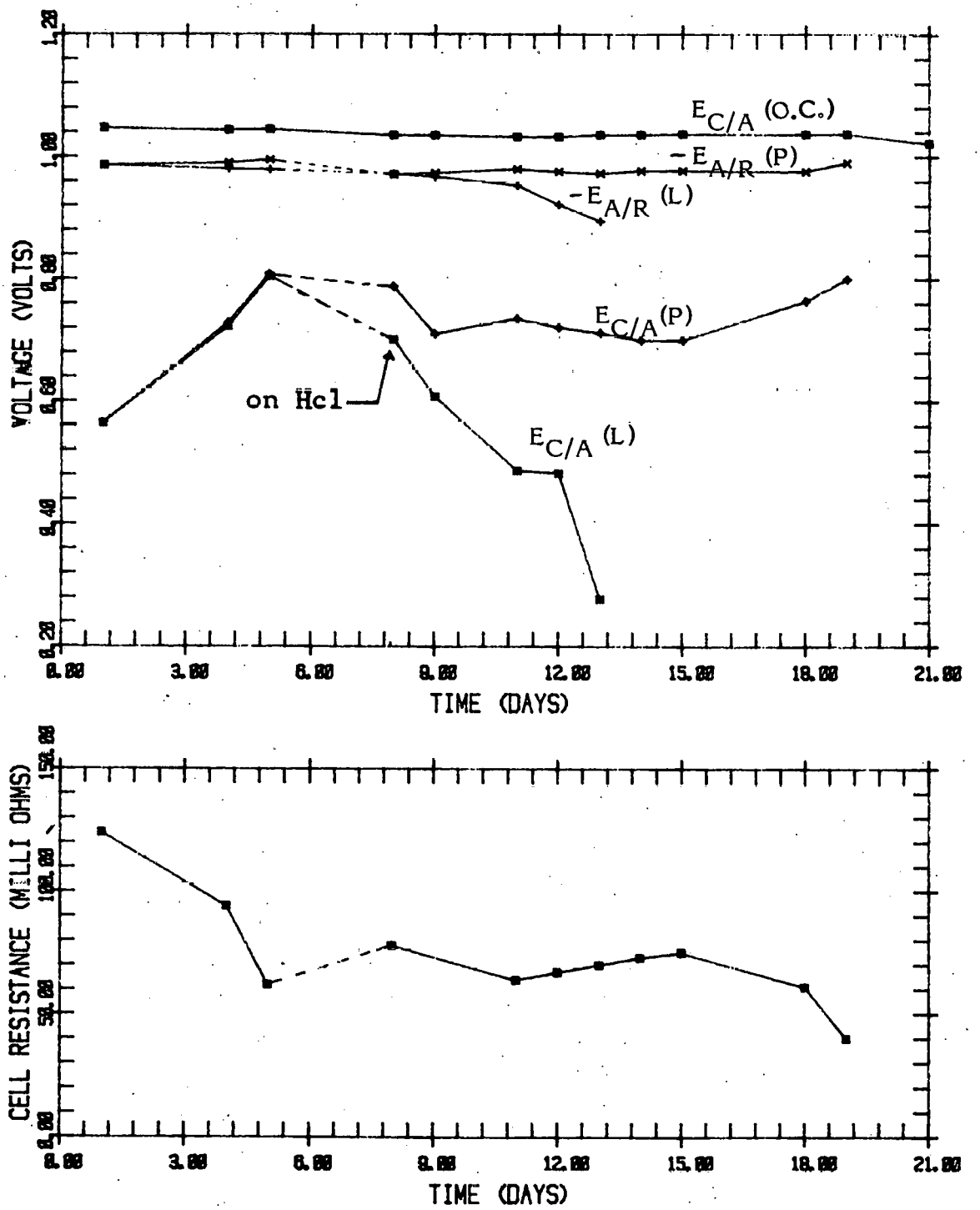

Figure 5.5 -- CRD049 Cell Performance With Time
Top: Cell Voltages At 2.2A vs Time; Bottom: Cell Resistance vs. Time

$$E_{C/A} = 1.022 - \frac{RT}{nF} \ln \frac{(.1177)(.1228)}{(.2228)(1)} + \ln \frac{1}{(.1486)^{1/2}(.30)} = 1.046\ V$$

With the dilution of the gases by 100 ppm HCl and .022 H_2O from the bubbler, the new theoretical open circuit becomes:

$$E_{C/A} = 1.022 - \frac{RT}{nF} \ln \frac{(.1359)(.1258)}{(.2146)} + \ln \frac{1}{(.1454)^{1/2}(.2935)} = 1.036\ V$$

Therefore, this 10 mv drop in open circuit is accounted for by the dilution of the gases and is not due to a mixed potential due to chloride take up by the tile. Figure 5.6 shows the current density as a function of time for this cell at a constant cell potential of 0.700 V from day 14 when the cell was switched to constant potential until day 21 when the cell was terminated.

It is obvious from Figures 5.5 and 5.6 that the HCl had a significant effect on cell performance. Furthermore, although the anode polarization did suffer slightly with time, the dramatic effect was on the cathode performance. By day 21 the effect of HCl could no longer be countered by a simple rest at open circuit. By day 21, even after an eight hour rest at open circuit, the cathode could not tolerate a 5 ma/cm^2 load. At this time the cell was shut down for post-mortem analysis.

No noticeable corrosion of either the nickel anode or wet seal area had occurred. There was, however, a build-up of corrosion products from the stainless steel hardware in the anode exit gas channel, and deterioration was observed in several areas of the cathode compartment. The stainless steel inserts from the cathode, shown in Figure 5.7, had undergone severe corrosion along with the entire stainless steel cathode chamber. The stainless steel current collector, also shown in Figure 5.7, had undergone corrosion to the extent of almost complete plugging of the gas passages with corrosion products. This corrosion was extensive at the inlet side of the current collector and extended for only a few millimeters downstream. The nickel-oxide cathode showed signs of changes in morphology and loss of adherence of particles. Samples of corrosion products, electrodes, and tile have been submitted for characterization and analysis.

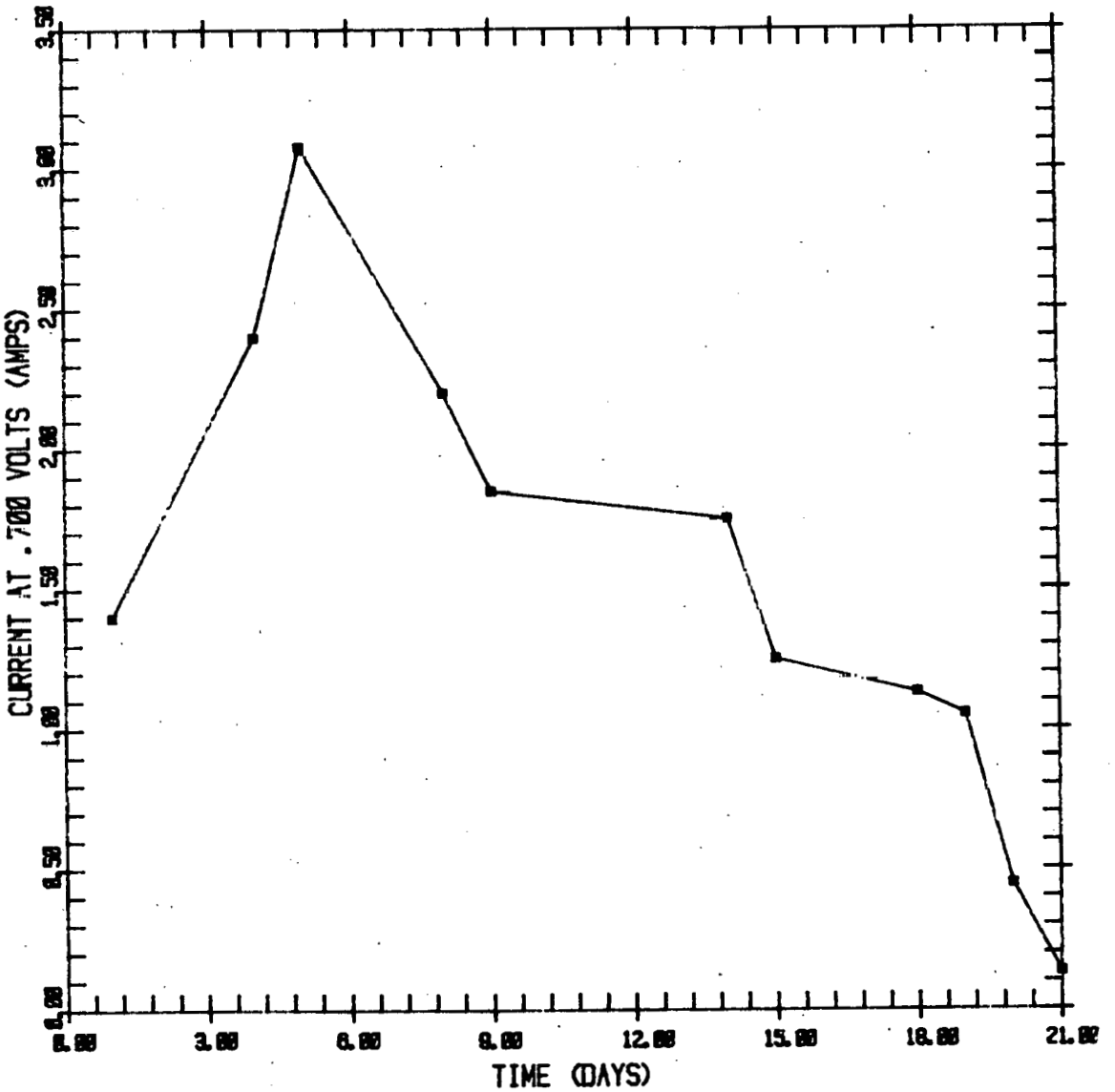

Figure 5.6 -- CRD049 Cell Performance; Cell Current At .700 Volts vs Time

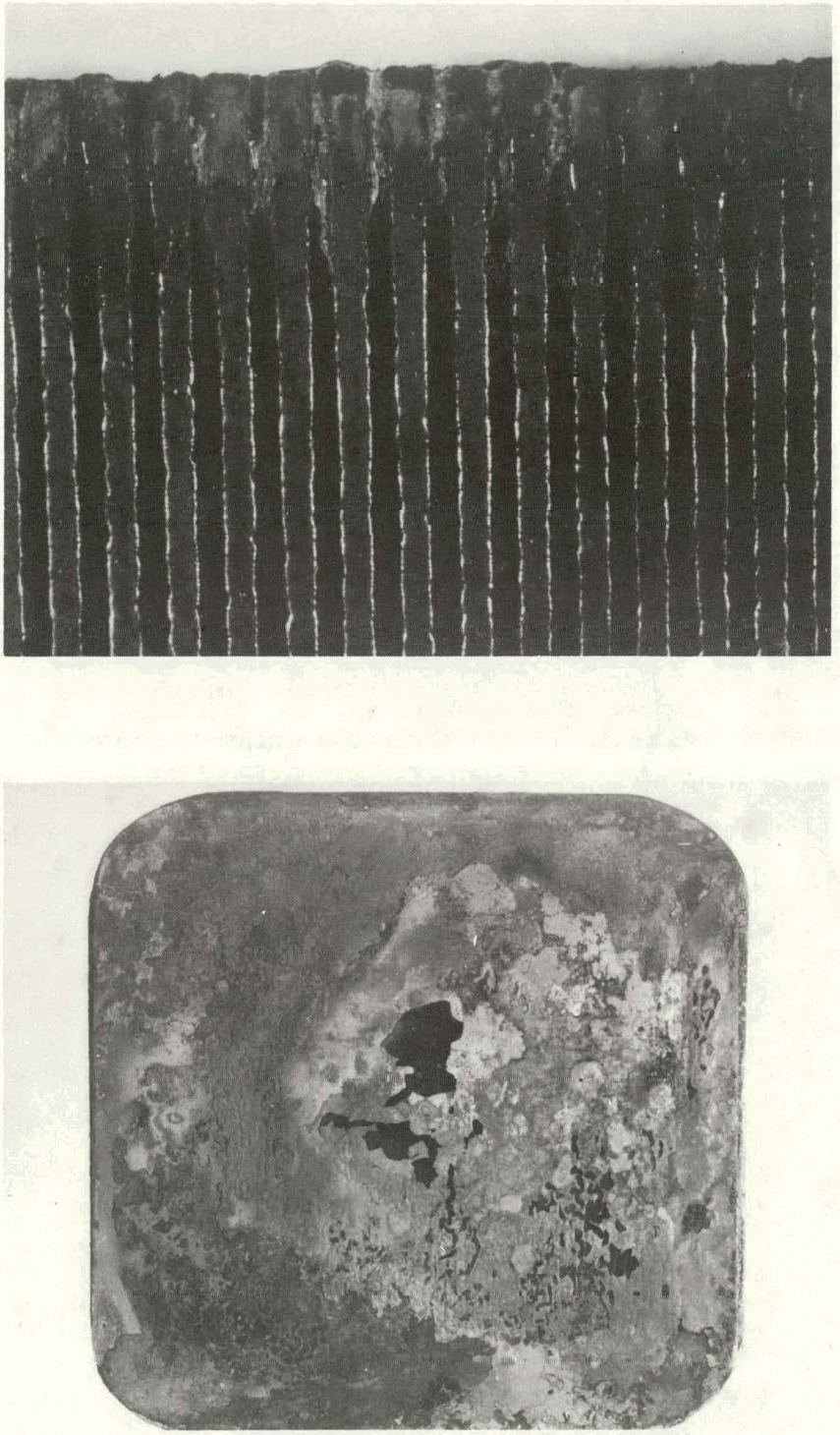

Figure 5.7 -- Top: CRD049 Stainless Steel Current Collector, Inlet Side Up (7.5X); Bottom: CRD049 Stainless Steel Insert (1.35X).

5.3.3 Discussion and Conclusions

It is apparent from the results of CRD049 that HCl has a severe effect upon cell performance when introduced to the cathode compartment. There are four major reactions which may be causing this loss in performance. The first involves take-up of the chlorine by the tile via the reaction:

$$K_2CO_3 + 2HCl = 2KCl + H_2O + CO_2 \qquad \Delta G_R = -49.455 \text{ kcal/mole}$$

This could explain the drop in resistance shown in Figure 5.5 at days 18 and 19. Although no thermodynamic data is available at present for the eutectic data, substantial take-up of the chlorine by the electrolyte would result in a change in open circuit potential versus our reference due to the difference in activity of the carbonate. Since no such change was apparent, except for day 21, either the eutectic data is closer to that for the Li_2CO_3 chlorination reaction:

$$Li_2CO_3 + 2HCl = 2LiCl + H_2O + CO_2 \qquad \Delta G_R = 12.196 \text{ kcal/mole}$$

or the chlorine was taken up by the hardware prior to contacting the electrolyte. Analysis of the tile for chlorine will be conducted.

The second possible effect of HCl at the cathode is chlorination of the stainless steel via the reaction:

$$Fe + 2HCl + 1/2\ O_2 = FeCl_2 + H_2O \qquad \Delta G_R = -54.080 \text{ kcal/mole}$$

At the operating condition of our cell, 15% oxygen, it would take only .2 ppm HCl to cause chlorination of the stainless steel, well below the 100 ppm value used.

The third possible reaction of HCl at the cathode is chlorination of the nickel oxide via

$$NiO + 2HCl = NiCl_2 + H_2O \qquad \Delta G_R = -1.747 \text{ kcal/mole}$$

At the operating conditions of our cathode, which ran on an oxidant gas containing 2.2% H_2O, it would require an HCl concentration of 23%, far above the 100 ppm HCl employed.

A final possible reaction of the HCl at the cathode is the formation of FeOCl via the reaction:

$$2\,Fe + 2\,HCl + 3/2\,O_2 = 2\,FeOCl + H_2O \qquad \Delta G_R = -137.213 \text{ (at } 527^{\circ}K)$$

Our cathode gas composition would, therefore, require an $a_{Cl} = 10^{-15}$. Although FeOCl decomposes at approximately 527°C, it is possible that since our cathode gas is not preheated that the severe corrosion at the inlet of the current collector plate is due to a localized lower temperature and formation of FeOCl.

Thus, chlorination of the stainless steel and chloride formation in the tile are possible explanations of the disastrous cell performance of CRD049. It is not known, at this time, whether a single mechanism or multiple mechanisms are responsible for this performance decay. It is clear, however, that these levels of HCl cannot be tolerated by operating MCFC. Future work in this area will be concentrated on determining the maximum tolerance limits of HCl and on the mechanisms of performance decay.

6. DEVELOPMENT OF SCALED-UP CELLS

6.1 LARGE MOLD FABRICATION

Due to delays from the supplier of H-21 tool steel, the fabrication of a 20" x 20" tile mold has been delayed. Completion of the mold is now expected in March.

6.2 SCALED-UP SINGLE CELL

The final design of the 10" x 10" hardware was completed and all component parts have been ordered. The final design differs from the preliminary design, reported previously (6.1), in the following areas:

- o A double bellows assembly replaces the diaphragm for seal and active area compression.
- o Current and voltage tabs have been added to the cell frame for alternate current and voltage connections.
- o Thin frame lower sheets have been added for improved cell flexibility (i.e., active vs. seal).

Problems with the fabrication of the insert design have forced a delay in the completion of the scale-up of cell hardware. The machine shop vendor found it impossible to fabricate the insert to our specifications within the constraints imposed on him by schedule and cost. To eliminate this bottleneck, the hardware inserts have been redesigned to facilitate manufacture while maintaining the original pressure drop and minimizing impact on diffusion and conductivity.

	Old Dimension (inches)		New Dimension (inches)		
	Groove Depth	Width	Land Width	Groove Depth	Width	Land Width
Anode .100	.020	.020	.050	.040	.040
Cathode .100	.015	.015	.050	.030	.040

The other parts of the scaled-up cell are nearing completion. However, the inserts will delay the availability of the complete cell assembly.

6.3 STACKABLE SCALE-UP DESIGN

Initial studies have been involved with the pressure drops in a 4' x 4' cell with 600-700 cells per stack. The approach here is to establish a configuration for the 4' x 4' cell operating at 150 PSIA and to scale down the developed concepts to a 10" x 10" cell operating at 15 PSIA.

The present flow field configuration in the boiler plate 10" x 10" design was evaluated for the 4' x 4' size at 150 PSIA and found to have only a 2" H_2O ΔP. Since the present 10" x 10" design does not lend itself to production, a significantly higher (2-3 PSI) ΔP may be required for optimum performance and cost effectiveness. Computer runs were made to estimate the pressure losses in a 45" x 45" cell in a 600-cell stack. The computer model assumed co-flow with multiple inlet and outlet stack manifolds, and a single sheet of material to form a bipolar collector or separator sheet between the anode and cathode sizes of adjacent cells. A bipolar collector with an overall formed height of .060 in. showed an average pressure loss of .16 psia in the flow field.

The major pressure loss design problem is in the cell manifold passages which distribute the reactant gases from the stack manifolds to the flow field adjacent to the cell active area. The pressure loss in the cell manifold passages is aggravated by the limited flow cross-sectional area and structural support for these passages. The use of multiple stack manifold passages relieves this problem.

The use of cross-flow virtually eliminates the need for cell manifold passages and multiple stack manifolds. Cross-flow may be an attractive approach in spite of the performance disadvantages.

Flow field evaluations will be continuing into the next reporting period as well as design of the 10" x 10" stackable cell.

7. REFERENCES

3.1 "Fuel Cell Research on Second-Generation Molten-Carbonate Systems", Quarterly Progress Report (1 January - 31 March 1978), July 1978, SAN-1735-2.

3.2 "Development of Molten Carbonate Fuel Cells For Power Generation", Quarterly Progress Report (15 May 1978-15 August), Sept. 1978, SRD-78-148.

3.3 "Development of Molten Carbonate Fuel Cells For Power Generation", Quarterly Progress Report (15 August-15 November 1978), Dec. 1978, SRD-79-006.

4.1 (Same as 3.3).